UNIVERSIDAD DE SEVILLA

FACULTAD DE FÍSICA

Departamento de Física Átomica, Molecular y Nuclear

Impact of the plasma resistivity in the tokamak SMART equilibria

Supervisor: Prof. Eleonora Viezzer

Carlos López Jiménez

Abstract

The Plasma Science and Fusion Technology group of the University of Sevilla is developing a new fusion device, the tokamak SMART, designed to study the behaviour of magnetically confined plasmas and train the next generation of plasma physicist and engineers. Plasma resistivity is a critical factor in determining the equilibrium properties of plasma, as it affects the plasma current density, magnetic field structure, and stability. This bachelor's thesis introduces a theoretical background on plasma dynamics, the tokamak SMART, and the numerical methods for computing plasma simulations.

FIESTA, a code package implemented in MATLAB, is used to model the impact of resistivity on the plasma equilibrium in the tokamak SMART. Two methods of modelling plasma resistivity will be examined, which include the Spitzer resistivity model alongside the neoclassical resistivity model.

Contents

1 Introduction

Over the last century, the standard of living has improved. Massive food production, operating industrial facilities, enabling instant communication, providing public and private transportation or supplying heating and electricity to households all come with the requirement of energy consumption. Fossil fuel has been a sine qua non to energy production since the Industrial Revolution, leading to climate change.

Humankind is now facing the consequences of unhindered greenhouse gas emission as the environment undergoes negative impacts, such as frequent droughts, rising sea levels, and increasing temperatures. If humanity does not deal with this issue in the near future, it may cause the self-destruction of our modern civilization. Energy demand is expected to more than double by 2050 [1], not only because of a better quality of life but also due to the steady growth of the population around the globe. Furthermore, the International Energy Agency proposes a net zero emissions by 2050 scenario, which maps out a way to achieve only an 1.5 °C increase in global average temperature. Therefore a radical change in the status quo of energy generation is critical in diving into this challenge. Only a clever portfolio of options that includes improvements in energy efficiency and clean, renewable sources would suffice for what the International Energy Agency advises [2].

The world's energy ultimately comes from the sun. The fossil fuels we consume come from trees that grew bathed in sunlight aeons ago. The energy from sun rays triggers evaporation, leading to cloud formation, and precipitation from these clouds provides us with hydro-power. Society is striving to reduce the need for burning coal, oil, or gas to generate electricity and is, instead, turning towards harnessing the power from the sun through the development of solar and wind power technologies. Despite their green and renewable origin, they may not be reliable enough -as it is impossible to control the weather conditions- to supply humanity with the energy demand the future awaits.

However, what if humanity created its *own* sun?

1.1 Nuclear fusion

Inspired by the nuclear reaction that occurs in stars, nuclear fusion, scientists have dreamed of recreating this phenomenon and benefiting from its dense energy-mass ratio. Firstly, a nucleus is a conglomerate of Z protons and N neutrons, A nucleons in total, bind all together through nuclear forces, at a very short range. The energy required to cluster all these particles into stability is known as the binding energy. The non-relativistic A-nucleon Hamiltonian is extraordinarily complex, in consequence, to do estimations on this energy, experimental data is required. From Einstein's mass-energy relation and the experimental masses of nuclei, it is possible to give a satisfactory result for the binding energy [3]:

$$BE({}^{\mathrm{A}}_{Z}\mathrm{X}) = Zm_p c^2 + Nm_n c^2 - M_N({}^{\mathrm{A}}_{Z}\mathrm{X})c^2 \ , \tag{1.1}$$

where m_p is proton mass, m_n is the neutron mass, M_N is the nucleus mass and c is the speed of light. Figure 1 shows the binding energy per nucleon as a function of nuclear mass, revealing that when two light nuclei are fused, the resulting nucleus has a larger binding energy. Recalling equation 1.1, the product of the reaction will have a lower mass and, in consequence, energy will be released. The equation to calculate this energy is simply:

$$Q = \sum_i M_i c^2 - \sum_f M_f \ . \tag{1.2}$$

When a deuterium nucleus fuses with a tritium nucleus, an α-particle is produced, and a neutron is released. The difference in mass between the reactants and the products will result in 17.6 MeV release per reaction:

$${}^{2}_{1}\mathrm{H} + {}^{3}_{1}\mathrm{H} \rightarrow {}^{4}_{2}\mathrm{He} + {}^{1}_{0}\mathrm{n} + 17.6 \text{ MeV} \ . \tag{1.3}$$

Doing a rough estimate, just 1kg of this fuel would release 10^8 kWh, sufficient to meet the energy demands of a 1GW (electric) power station for a day[5].

Let us consider the three main advantages fusion power delivers as an energy source: fuel reserves, environmental impact, and safety. In ocean water, there is one atom of deuterium for every 6700 atoms of hydrogen. After extracting all the deuterium in the seven seas, it could be

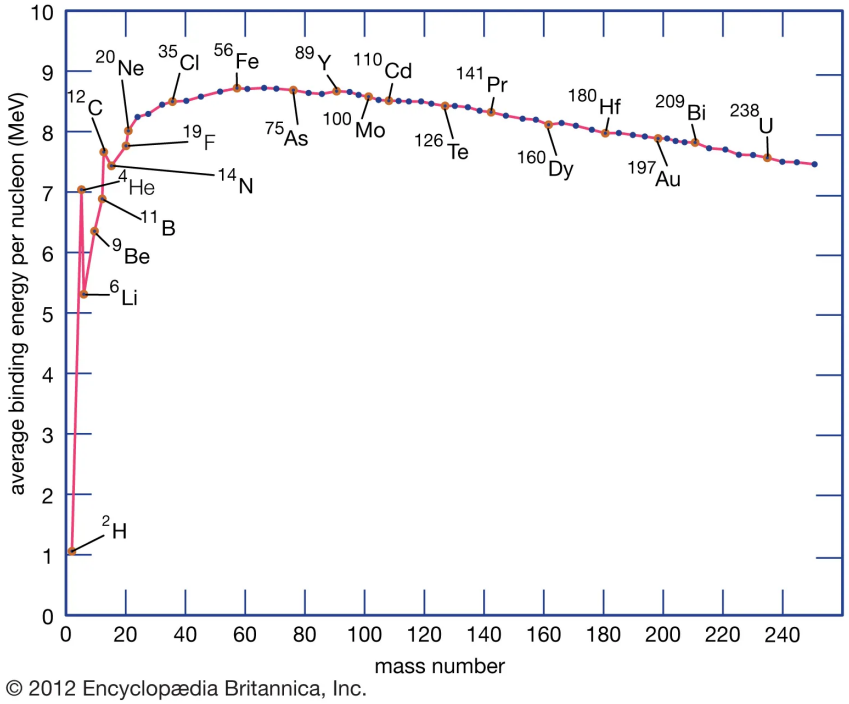

Figure 1: Nuclear binding energy per nucleon as a function of the nuclear mass number. Source: [4].

generated enough energy to supply the earth's demand for about two thousand million years [6]. Likewise, fusion reactions produce no CO_2, other greenhouse emissions or harmful chemicals into the atmosphere. The radiated α-particles, once they de-ionize, are nothing more than inert helium gas. The only environmental problem may arise from the high-energy neutrons. Thus, they are captured in the fusion blanket, making them innocuous to the public. Finally, unlike its counterpart nuclear reaction, *fission*, the possibility of radioactive meltdown is out of the table. The fusion process does not involve a chain reaction or the production of long-lived radioactive waste. Instead, fuel is constantly fed into the reactor allowing it to be consumed as needed. Given the situation of critical failure, the reactants would cool down, stopping the fusion reaction safely.

So what is holding scientists and engineers back? Well, the almost limitless deuterium is constricted by the short supply of tritium, which does not occur naturally on the earth. In order to bypass this issue, the emitted neutrons breed an isotope of lithium, ^{6}Li, found as a component of the fusion blanket, producing the required tritium. The ^{6}Li reserves cap the overall source for deuterium-tritium fusion. Geological estimates predict approximately 20000 years of inexpensive ^{6}Li available. It is expected that before ^{6}Li is exhausted, other fusion reactions, such as deuterium-

deuterium, could be performed. On the other hand, the inertia has to overcome the electric repulsion of ions with like charges. Stars in the universe circumvent this problem thanks to their extreme gravitational domain yielding tremendous pressures. In laboratories, the reactants ought to be heated up to 10 keV [5], ten times hotter than the core of the sun. At these temperatures, the reactants -deuterium and tritium- fully ionize and become plasma. When deuterium and tritium particles reach these temperatures, by quantum mechanical tunnelling, the Coulomb barrier is overcome. This is known as *thermonuclear* fusion. Not only that, the amount of power released by the nuclear reaction must exceed the power supplied to the fusion reactor, in other words:

$$Q = \frac{P_{fusion}}{P_{supplied}} > 1 \ . \tag{1.4}$$

To achieve this requires clever engineering. As plasma cools down, power is lost irremediably. This power loss must be replenished by plasma heating. The amount of power lost is depicted by an energy confinement time [5], given the plasma energy W:

$$P_L = \frac{W}{\tau_E} \ , \tag{1.5}$$

where P_L is the power loss and τ_E the energy confinement time. The plasma energy can be calculated knowing that, if the average energy of plasma particles is $\frac{3}{2}k_BT$ -where k_B is the Boltzmann's constant, n is the electron density and T is the electron temperature- and there is as many electrons as ions, the plasma energy per unit volume is $3nk_BT$. Therefore:

$$W = \int 3nk_BTd^3x = 3nk_BTV \ , \tag{1.6}$$

In principle, to sustain the reaction, the power supplied must be equal to the power lost $P_S = P_L$, where P_S is the supplied power. However, the α-particles released by the reaction should be taken into account. Because of their charged nature, through Coulomb collisions, α particles transfer their energy to the plasma, giving rise to what is known as α-heating. Reconfiguring the equation to, $P_L = P_S + P_\alpha$, where P_α is the power transferred by the α particles. The α-particle heating per unit volume is:

$$p_\alpha = \frac{1}{4}n^2\langle\sigma v\rangle E_\alpha \ , \tag{1.7}$$

giving a total α-particle heating of

$$P_\alpha = \int p_\alpha d^3x = \frac{1}{4} n^2 \langle \sigma v \rangle E_\alpha V \ , \tag{1.8}$$

where n is the particle density, $\langle \sigma v \rangle$ is the average cross section of the reaction times the velocity [5], E_α the energy of the α-particle and V the total volume. The final power balance is given by,

$$P_S + \frac{1}{4} n^2 \langle \sigma v \rangle E_\alpha V = \frac{3 n k_B T V}{\tau_E} \tag{1.9}$$

As the deuterium-tritium plasma is heated to thermonuclear conditions, α-particle heating becomes a progressively larger portion of the total heating. With the right confinement conditions, a critical point is reached where the plasma temperature can be maintained by its internal heating alone. This critical point, analogous to the combustion of fossil fuels, is referred to as *ignition*. It is possible to deduce this condition thanks to equation 1.9:

$$n \tau_E > \frac{12 T}{\langle \sigma v \rangle E_\alpha} \ . \tag{1.10}$$

This is known as the *Lawson criterion*. Using some known results, this inequality becomes:

$$n k_B T \tau_E > 3 \cdot 10^{21} m^{-3} \ keV s \tag{1.11}$$

This condition could be reached for example by $n = 10^{20} m^{-3}$, $k_B T = 10 keV$ and $\tau_E = 3 s$ [5].

1.2 Aim of the work

This bachelor's thesis aims to delve into the intriguing realm of plasma physics and investigate the impact of plasma resistivity in the equilibrium of the tokamak SMART. Tokamaks are advanced devices designed for controlled nuclear fusion experiments. Understanding the dynamics within these toroidal magnetic confinement devices is paramount to harnessing the power of nuclear fusion. Plasma resistivity, a fundamental parameter in plasma physics, plays a pivotal role in shaping the behaviour of a tokamak's plasma. The research on the importance of plasma resistivity will be made through the numerical solver, FIESTA.

FIESTA is a code package that simulates plasma equilibria in the tokamak SMART. At first, this computational tool used the Spitzer resistivity model when performing plasma simulations. Thus, during this bachelor's thesis, the neoclassical resistivity model will be implemented into the code environment, hoping to give an interesting comparison between the two models and, consequently, find insight into the impact of the plasma resistivity in the tokamak SMART equilibria. The objectives for this project go as follows,

- Understand how plasma is confined through magnetic fields.
- Learn to use the FIESTA code in the Matlab environment.
- Create a new code that implements the neoclassical resistivity model in FIESTA.
- Compare simulations made with the different resistivity models, Spitzer and neoclassical.

2 Theoretical background

2.1 Plasma confinement

As one can expect, such high temperatures impede ordinary means to confine the plasma. Two primary approaches exist for containing plasma: *magnetic confinement* and *inertial fusion*. Given that this bachelor's thesis focuses on the tokamak SMART, the theoretical background necessary to comprehend the magnetic confinement approach will covered throughout this chapter. First and foremost, what is *plasma*?

Paraphrasing Francis. F. Chen[7], '*a plasma is a quasineutral gas of charged and neutral particles which exhibits collective behavior*'. Its components have many of the properties of an ordinary gas, such as temperature, density or pressure. However, they exhibit two characteristic properties [5]. The enormous electric charge density of the two species leads to a vice-like restoring force at the appearance of any substantial separation, and the outcome is ion and electron charge densities being almost equal in plasma in equilibrium. On the other hand, plasma can conduct an electric current, which arises from the relative motion between ions and electrons. In a tokamak, the plasma current is responsible for a substantial portion of the magnetic field. When this current crosses the magnetic field, it creates a magnetic force which can balance the plasma internal pressure, reaching the equilibrium.

What is *collective behaviour*? Plasmas present an enormous variety of collective dynamical modes that arise due to the large number of charged particles that interact with each other through electromagnetic forces. These interactions result in various phenomena, such as plasma oscillations, waves, instabilities, etc. In order to be dominant, electromagnetic interactions must have a *global* effect on plasma dynamics. Ergo, one-to-one Coulomb interaction must play a minor role. Recalling the similarities between plasma and an ordinary gas, let us consider the forces acting on a molecule of air. Air molecules, thanks to their neutrality and low mass, experience negligible electromagnetic and gravitational forces, allowing them to move free until they collide with another molecule. These collisions are the primary factors governing the motion of gas particles. When applying a macroscopic force to a neutral gas, like sound waves from a speaker, they transmit to individual atoms through collisions. However, this situation is entirely different in plasma, composed of charged particles.

The movement of these charged particles can lead to accumulations of charge, creating electric fields. Moreover, this motion gives rise to electric currents and, consequently, magnetic fields. These electric and magnetic fields influence the trajectories of other charged particles, even those found far away from the source of the original motion, resulting in complex and interconnected behaviour within the plasma. Let us consider two slightly charged regions within a distance r. The Coulomb force between the two regions, A and B, decreases as $1/r^2$. Nevertheless, for a given solid angle (i.e. $\Delta r/r$=constant), the volume of plasma in B that can impact A increases as r^3. Therefore, regions of plasma wield a force on one another even at large distances [7], giving rise to a large repertoire of possible motions.

2.1.1 Debye shielding

As mentioned before, one of the properties correspond to the quasineutrality nature of a plasma in equilibrium. To illustrate this, let us assume an initially neutral plasma, i.e., $n_i = n_e = n_0$, where a test charge is placed. Poisson's equation yields:

$$\nabla^2\phi(\vec{r}) = -\frac{\rho(\vec{r})}{\epsilon_0} \,, \tag{2.1}$$

where ϕ is the electric potential, $\rho(\vec{r})$ the charge density and ϵ_0 the vacuum permittivity. Thus, applied to the system becomes:

$$\nabla^2\phi(\vec{r}) = -\frac{1}{\epsilon_0}[q_t\delta(\vec{r}) + (n_i(\vec{r}) - n_e(\vec{r}))e] \,, \tag{2.2}$$

where q_t is the test charge and $n_i(\vec{r})$, $n_e(\vec{r})$ the ion and electron charge densities, respectively. As a first approximation, assuming that ions are so heavy -compared to the electrons-, they will not budge in the presence of the test charge, behaving as a fixed background. On the other hand, the electron density responds to the Maxwell-Boltzmann law in the pressence of a potential $q\phi$[7]:

$$f(u) = Aexp\left(-\frac{1/2mu^2 + q\phi(\vec{r})}{k_B T}\right) \,, \tag{2.3}$$

where $f(u)$ is the electron velocity distribution function, u is the electron velocity and A is a normalization constant. Integrating $f(u)$ over u, setting $q = -e$, and considering that

$n_e(\phi \to 0) = n_0$ [7], the electron distribution is given as:

$$n_e = n_0 \exp\left(\frac{e\phi(\vec{r})}{k_B T}\right) . \tag{2.4}$$

Applying equation 2.4 into the differential equation 2.2 gives:

$$\nabla^2\phi(\vec{r}) = -\frac{1}{\epsilon_0}\left[q_t\delta(\vec{r}) + en_0 - en_0 \exp\left(\frac{e\phi(\vec{r})}{k_B T}\right)\right] . \tag{2.5}$$

From now on, $k_B T \to T$[1]. Considering a small perturbation, $\frac{e\phi}{T} << 1$, it is possible to do first-order Taylor expansion to solve the equation above:

$$-\frac{1}{\epsilon_0}\left[q_t\delta(\vec{r}) + en_0 - en_0 \exp\left(\frac{e\phi(\vec{r})}{T}\right)\right] \approx -\frac{q_t}{\epsilon_0}\delta(\vec{r}) + \frac{e^2 n_0}{\epsilon_0 T}\phi(\vec{r}), \tag{2.6}$$

$$\nabla^2\phi(\vec{r}) - \frac{1}{\lambda_D^2}\phi = -\frac{q_t}{\epsilon_0}\delta(\vec{r}) . \tag{2.7}$$

Defining $\lambda_D = \sqrt{\frac{T\epsilon_0}{e^2 n_0}}$ as the Debye length. The solution to this partial differential equation is:

$$\phi(r) = \frac{q_t}{4\pi\epsilon_0 r} \exp\left(\frac{-r}{\lambda_D}\right) \tag{2.8}$$

Upon a closer examination of the solution, the plasma screens the electrostatic potential generated by the test charge, showing that small perturbations to the charge density and potential in plasma tend to fall off with distances superior to the Debye length. This is known as *Debye shielding*. Systems with adequate scales will be broadly neutral, i.e., $L^3 >> \lambda_D^3$, where L^3 is the plasma volume.

2.1.2 Plasma frequency

To depict the collective aspect of plasma, it should first be establish the plasma frequency and collision frequency. Let us consider displaced layers of electrons as shown in figure 2. As stated

[1] It is usual in plasma physics to redefine temperatures in energy units, absorbing the Boltzmann constant and simplifying the notation.

above, because of their larger mass, ions are fixed in the background. The positive charges in the figure represent the depletion of electrons from the affected layers. The resulting electric field appears below the illustration. Consequently, the negative charges will flow into the positively charged regions. This motion would be cyclical, resulting in plasma oscillations.

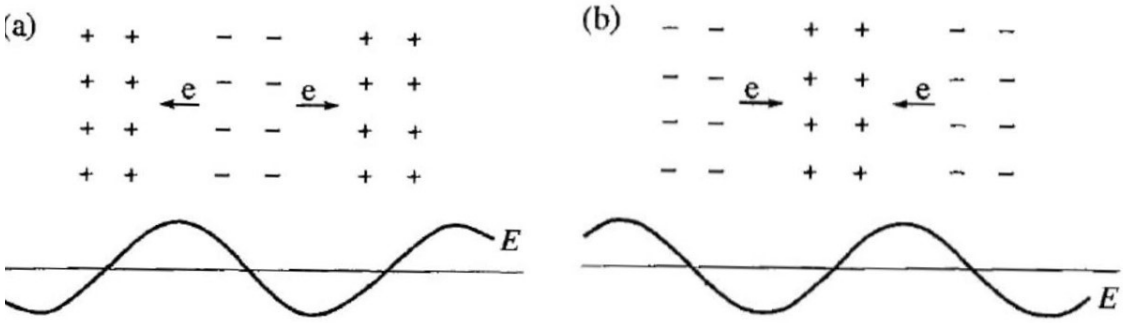

Figure 2: a) Displaced layers of electrons creates a restoring force, followed by acceleration, b) after half-cycle the charges change places; Source:[5]

The fluid motion equation for a cold plasma is [5]:

$$m_e \frac{\partial \vec{v}}{\partial t} = -e\vec{E} \ , \tag{2.9}$$

where m_e is the electron mass, $\vec{v}$ the fluid electron velocity and $\vec{E}$ the electric field. Assuming a small density perturbation n', Gauss' law states:

$$\nabla \cdot \vec{E} = -\frac{en'(\vec{r})}{\epsilon_0} \ . \tag{2.10}$$

Taking divergence on 2.9 and using the result from 2.10 gives:

$$m_e \frac{\partial}{\partial t} \nabla \cdot \vec{v} = -\frac{en'(\vec{r})}{\epsilon_0} \ . \tag{2.11}$$

On the other hand, the fluid continuity equation is [5]:

$$\frac{\partial n(\vec{r})}{\partial t} = -\nabla \cdot (n(\vec{r})\, \vec{v}) \ . \tag{2.12}$$

It is possible to linearize[2] this equation taking the original approximation of a small perturbation n':

$$n(\vec{r}) \approx n_0 + n'(\vec{r}) \ , \tag{2.13}$$

thus, applied to the differential equation

$$\frac{\partial n'(\vec{r})}{\partial t} = -n(\vec{r})\, \nabla \cdot \vec{v} \ . \tag{2.14}$$

Then, applying the result form 2.14 into 2.11 gives the equation of plasma oscillations:

$$\frac{\partial^2 n'(\vec{r})}{\partial t^2} = -\omega_p^2 n'(\vec{r}) \ , \tag{2.15}$$

where $\omega_p = \sqrt{\dfrac{ne^2}{\epsilon_0 m_e}}$ is the electron plasma frequency.

Let us now do a rough estimate on Coulomb collisions. Consider an electron that undergoes a *major*[3] angular change from its trajectory when interacting with another electron which occurs when the Coulomb interaction energy is comparable to the kinetic energy, i.e.:

$$\frac{E_C}{E_K} \sim \frac{e^2}{4\pi\epsilon_0 m_e b v_{th,e}^2} \sim 1 \ , \tag{2.16}$$

where b is the impact parameter and $v_{th,e}$ is the average thermal electron velocity. It is possible to identify a cross-section, $\sigma_0 = \pi b^2$, from the impact parameter and apply it to the following approximate formula for the frequency of collisions [9]:

$$\nu_c = n_e v_{th,e} \sigma_0 \ , \tag{2.17}$$

Let us compare the plasma frequency and the frequency of collisions. Rewriting the plasma frequency accordingly:

$$\omega_p = \sqrt{\frac{ne^2}{\epsilon_0 T_e}} \sqrt{\frac{T_e}{m_e}} = \frac{v_{th,e}}{\lambda_D} \ , \tag{2.18}$$

[2] $\nabla n'(\vec{r}) \propto \nabla^2 \vec{E} + \nabla \times (\nabla \times \vec{E})$, being a second order term, thus can be approximated to zero.
[3] For a further analysis, consult [8], section 1.8, 'Collisions'

and using the results from 2.16 and the definition of the Debye length gives the following ratio:

$$\frac{\omega_p}{\nu_c} = 16\pi N_D >> 1 \ , \tag{2.19}$$

showing that the collective effects overcome one-to-one interactions[4]. $N_D \sim n_e \lambda_D^3$ which fulfills 2.19 in tokamak plasmas [9].

2.1.3 Motion of charged particles

Analyzing plasma dynamics can be complex due to the interplay of fluid-like behavior and collective Coulomb interaction. Studying individual particle responses to electric and magnetic fields is crucial for understanding plasma physics. The foundation for establishing the single-particle model is Newton-Lorentz's equation [10], which describes the motion of a particle with mass m and charge q in the presence of an electric field $\vec{E}$ and a magnetic field $\vec{B}$:

$$m\frac{d\vec{v}}{dt} = q(\vec{E} + \vec{v} \times \vec{B}) \ . \tag{2.20}$$

A wise approach to solve this differential equation, given $\vec{E}(\vec{r}, t)$ and $\vec{B}(\vec{r}, t)$, would be from the simplest case and gradually start generalising. The simplest case is the one with a uniform magnetic field, let us say in the z direction. A charged particle will obey 2.20:

$$m\frac{d\vec{v}}{dt} = q\vec{v} \times \vec{B}_0 \ . \tag{2.21}$$

This can be rewritten into a Cartesian explicit form:

$$\frac{dv_x}{dt} = \omega_c v_y \ , \qquad \frac{dv_y}{dt} = -\omega_c v_x \ , \qquad \frac{dv_z}{dt} = 0 \ , \tag{2.22}$$

where $\omega_c = \dfrac{qB_0}{m}$ is the cyclotron frequency. Easily one can deduce that the velocity along the magnetic field lines remains constant. On the other hand, integrating 2.22 gives the following solutions:

$$v_x = v_\perp sin(\omega_c t) \ , \qquad v_y = v_\perp cos(\omega_c t) \tag{2.23}$$

[4] In subsection 2.3.1, figure 8 depicts a collision between two charged particles with an impact parameter r

where $v_\perp$ is the module of the perpendicular component -with respect to the magnetic field- of the particle velocity.

Then, the trajectory of the particle would be [5]:

$$x = -\rho_L cos(\omega_c t) \ , \qquad y = \rho_L sin(\omega_c t) \ , \qquad z = v_z t \ . \tag{2.24}$$

where $\rho_L = \dfrac{m v_\perp}{q B_0}$ is the Larmor radius. From these equations an helical motion arises, traced around the *guiding centre* -the axis of the helix-, as seen in figure 3. The direction of rotation depends on the sign of the charge. Ions rotate anticlockwise, electrons do the opposite. In the end, the current carried by the plasma is always in such a direction as to reduce the magnetic field, i.e. plasma is a diamagnetic fluid.

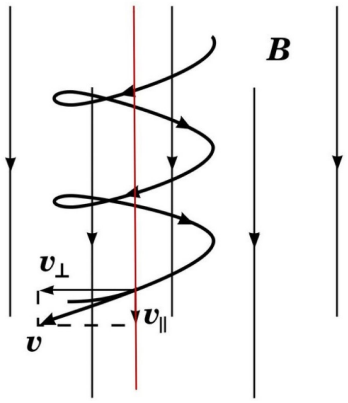

Figure 3: Trajectory of a charged particle in an uniform magnetic field; Source: [11].

The presence of an electric field or non-uniform magnetic fields will add complexity to the basic motion previously described. Throughout this section, the nuances of these added effects are described. In order to ease the analysis of the new trajectories, the velocity of the particle is decomposed into parallel and perpendicular with respect to the magnetic field:

$$\vec{v} = \vec{v_\parallel} + \vec{v_\perp} \ , \tag{2.25}$$

Acceleration due to $\vec{E}_\parallel$

A parallel electric field will, thanks to the Coulomb force, accelerate the particle along the guiding centre, as shown in 2.26:

$$m\frac{d\vec{v_\parallel}}{dt} = q\vec{E}_\parallel \ . \tag{2.26}$$

[5] Assuming $\vec{r} = (0, 0, 0)$ as an initial condition

$\vec{E} \times \vec{B}$ drift

The presence of an electrical field perpendicular to the magnetic field, for example, $\vec{E} = (0, E, 0)$ and $\vec{B} = (0, 0, B)$, exerts a drift perpendicular to both fields onto the particle, to see this, Cartesian coordinates are applied:

$$\frac{dv_x}{dt} = \omega_c v_y \ , \qquad \frac{dv_y}{dt} = \frac{q}{m}E - \omega_c v_x \ , \qquad \frac{dv_z}{dt} = 0 \ . \tag{2.27}$$

The solution to these equations can be written as:

$$v_x = v_\perp sin(\omega_c t) + \frac{E}{B} \ , \qquad v_y = v_\perp cos(\omega_c t) \ , \qquad v_z = v_\parallel \ . \tag{2.28}$$

This drift is independent of the charge, mass and energy of the particle, affecting all particles in the plasma equally. The perpendicular electric field, is frame dependent, so it is possible to find a gauge where the orbit would simply be helical [5]:

$$\vec{E} + \vec{v_f} \times \vec{B} \ . \tag{2.29}$$

Crossing equation 2.29 with $\vec{B}$ leads to a definition for the drift velocity. This is the speed at which the gyro centre drifts away:

$$\vec{v_d} = \frac{\vec{E} \times \vec{B}}{B^2} \ . \tag{2.30}$$

This result can be extended to any external force applied to the particle just by substituting $q\vec{E}$ in equations 2.27 by a general force $\vec{F}$, which results in:

$$\vec{v_d} = \frac{\vec{F} \times \vec{B}}{qB} \tag{2.31}$$

Accelartion due to $\nabla_\parallel B$

In this example cylindrical coordinates are used, where r is the radial distance, ϕ is the azimuth angle and z is the axial coordinate. Let us consider a more complex magnetic field, that varies along space. Under the presence of a gradient parallel to $\vec{B}$, a force in the same direction of the gyro-centre appears[7]. In this scenario, the magnetic field is primarily oriented in the z-direction and varies in magnitude along the z-direction. This magnetic field is axisymmetric, meaning it

has no component in the ϕ-direction ($B_\phi = 0$) and no variation with respect to the ϕ angle ($\frac{\partial \vec{B}}{\partial \phi} = 0$). However, because the magnetic field lines converge and diverge, there must be a radial component, B_r. Considering Newton-Lorentz's law:

$$\vec{F} = q(\vec{v} \times \vec{B}) \, , \tag{2.32}$$

that, applying cylindrical coordinates, leaves us with:

$$\begin{aligned} F_r &= q(v_\theta B_z - \cancel{v_z B_\phi}) \, , \\ F_\phi &= q(v_z B_r - v_r B_z) \, , \\ F_z &= q(\cancel{v_r B_\phi} - v_\phi B_r) \, . \end{aligned} \tag{2.33}$$

Equations 2.33 give rise to three different motions, the already studied Larmor orbits, an azimuthal force that provokes a drift in the radial direction -making the guiding centre to follow the lines of force [7]- and the $\nabla_\parallel B$ acceleration.

It is possible to deduce B_r from $\nabla \cdot \vec{B} = 0$:

$$\frac{1}{r}\frac{\partial}{\partial r}(rB_r) + \frac{\partial B_z}{\partial z} = 0; \, . \tag{2.34}$$

Provided that $\frac{\partial B_z}{\partial z}$ is approximately independent from r, it is possible to give an estimation for B_r, solving equation 2.34:

$$\begin{aligned} rB_r = -\int_0^r r\frac{\partial B_z}{\partial z} dr \quad &\approx -\frac{r^2}{2}\left[\frac{\partial B_z}{\partial z}\right]_{r=0} \\ B_r = -\frac{r}{2}\left[\frac{\partial B_z}{\partial z}\right]_{r=0} & \end{aligned} \tag{2.35}$$

Therefore, the force that particles experiment under this circumstances is:

$$F_z = \frac{qv_\phi r}{2}\frac{\partial B_z}{\partial z} \, . \tag{2.36}$$

Selecting a particle whose guiding centre lies on the axis of the frame of reference and given that particles gyrates in opposites directions depending on the nature of the charges, the equation

becomes:

$$-\frac{mv_{\perp}^2}{2B}\frac{\partial B_z}{\partial z} \ . \tag{2.37}$$

It is possible generalize the result to:

$$\vec{F}_{\parallel} = -\mu\nabla_{\parallel}B \ , \tag{2.38}$$

where $\mu = \dfrac{mv_{\perp}^2}{2B}$, defined as the magnetic moment of a charged particle.

$\nabla B \perp \vec{B}$ drift

It can be proven that in a magnetic field with a perpendicular gradient the particle Larmor radius would be smaller where the magnetic field is stronger, leading to a drift perpendicular to both, magnetic field and its gradient [5]. The drift velocity is:

$$\vec{v}_{\nabla B} = \frac{mv_{\perp}^2}{2qB^3}(\vec{B}\times\nabla B) \ . \tag{2.39}$$

For a more in depth explanation consult [5]. This drift is charge dependent, making ions and electrons drift in opposite directions.

Curvature drift

Particles moving in a curved $\vec{B}$ tend to follow the field lines as motion across $\vec{B}$ is resisted [9]. Let us make the assumption that the magnetic field lines are curved with a constant radius of curvature, R_c, and the magnitude of the magnetic field, B, remains constant. It's important to note that such a magnetic field configuration doesn't conform to Maxwell's equations in a vacuum. In practical situations, the ∇B drift is typically added to this effect. A centrifugal force would be felt by the particles trying to follow the magnetic lines:

$$\vec{F}_c = \frac{mv_{\parallel}^2}{R_c^2}\vec{R}_c \ , \tag{2.40}$$

in consequence, a drift will emerge

$$\vec{v}_c = \frac{mv_{\parallel}^2}{qB^2}\frac{\vec{R}_c\times\vec{B}}{R_c^2} \ . \tag{2.41}$$

It is important to add the contribution of the ∇B drift that comes with the decrease of B with the radius is taken into account. It can be proven that in this case the drift would have the same direction and would take the following form:

$$\vec{v}_{\nabla B} = \frac{m v_\perp^2}{2q} \frac{\vec{R}_c \times \vec{B}}{R_c^2 B^2} \ . \tag{2.42}$$

For a more in depth explanation consult [7]. The total drift would be:

$$\vec{v}_c + \vec{v}_{\nabla B} = \frac{m}{q} \frac{\vec{R}_c \times \vec{B}}{R_c^2 B^2} (v_\parallel^2 + \frac{1}{2} v_\perp^2) \ . \tag{2.43}$$

2.1.4 Torodial magnetic confinement

In the previous subsection, the dynamics of charged particles in plasma were explored, including their various drift motions. This subsection focuses on the essential concept of toroidal magnetic confinement[6]. Shaping the magnetic field lines into a torus removes the end losses, trapping particles more efficiently. These kinds of confinement schemes are known as tokamaks and stellarators. However, everything comes with a price. Closing the magnetic lines brings inhomogeneity and curvature to the magnetic field. This gives rise to drifts to the guiding centre of the helical orbits. In a magnetic confinement device like a tokamak, the toroidal field is generated by field coils with a greater winding density on the inner edge of the torus than the outer edge. Thus, the magnetic field will be radially inhomogeneous. This field can be computed using Ampere's law [10]:

$$\oint_\Gamma \vec{B} d\vec{l} = 2\pi \mu_0 r B_\phi(r) r = nI \ , \tag{2.44}$$

where, n is the number of windings, I the current that goes through them and, Γ the integration path which follows a field line of radius r which encloses the total current nI. This means that the toroidal magnetic flux density decreases radially as:

$$B_\phi = \frac{\mu_0 nI}{2\pi r} \ . \tag{2.45}$$

[6] From now on, this text will make use of cylindrical coordinates, applied on a torus, see appendix A.

In a purely toroidal field two drifts are present, *curvature drift* and ∇B *drift*. As seen in equation 2.43, both contributions add in the same direction. Furthermore, this drift is charge dependent, creating a region of depletion charges, leading to an electrical field which will produce another drift, the $\vec{E} \times B$ *drift*, ejecting the plasma out of the torus, along the radial direction, as seen in figure 4a. Clearly, a toroidal field will not confine plasma. In order to counter the outward

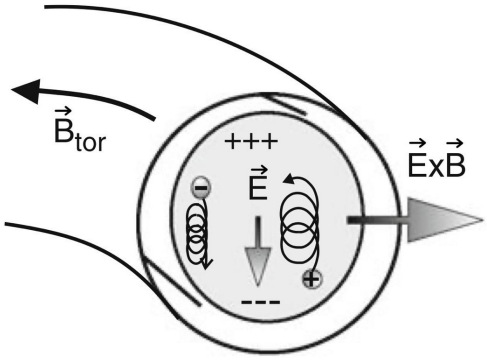

(a) An electric field appears due the separation of the charges, making particles drift away from the torus, Source: [10].

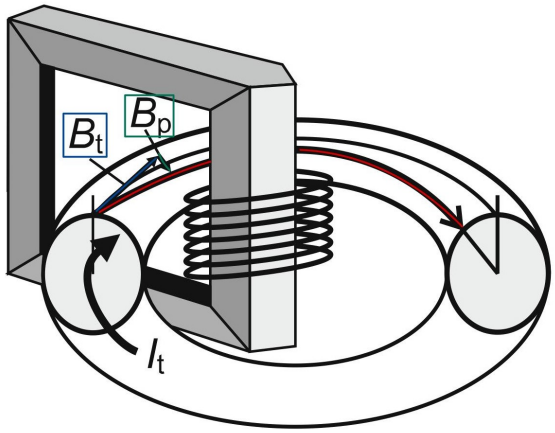

(b) Using and induced toroidal current a poloidal field is created, twisting the magnetic field lines. Only one yoke of the transformer is shown. Source: [10].

Figure 4: Poloidal magnetic flux optimized equilibrium.

drift of plasma, the toroidal magnetic field lines are twisted. This twist causes field lines from the outer edge to move inside after a few revolutions around the torus' major axis. This rotational transformation is achieved by adding a poloidal magnetic field, denoted as B_θ.[7] In a tokamak, this poloidal field is generated by inducing a toroidal current I_ϕ, within the plasma ring. To achieve this, a central solenoid creates a magnetic field that, following Maxwell-Faraday's law, i.e.:

$$\nabla \times \vec{E} = -\frac{\partial \vec{B}}{\partial t} \,, \tag{2.46}$$

will induce a toroidal electric field inside the plasma, thus inducing a current density. To maintain this current, the magnetic field must have an adequate time dependence. This is achieved through a changing solenoid current. Figure 4b illustrates this principle in a tokamak, showing how field lines are twisted.

[7] Check appendix A for a reference on toroidal coordinates

2.1.5 SMART overview

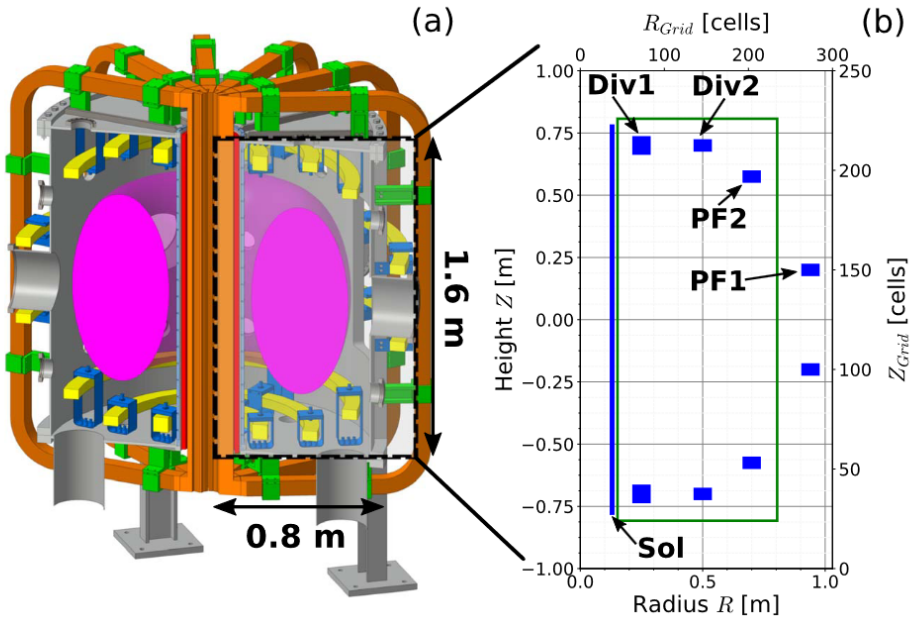

Figure 5: This figure shows a 3D section of the vessel and coil geometry a) and a 2D graph, locating the solenoid, PFC and Div coils more clearly. The vacuum vessel is depicted in grey, toroidal field coils (TFC) in orange, poloidal field coils (PFC), and divertor coils (Div) in yellow, the solenoid (Sol) in red, and support structures in blue and green. Source: [12].

The SMART is a spherical tokamak designed to achieve low aspect ratio plasma[8]. The device consists of a 0.8 m radius by 1.6 m height stainless steel (AISI 316 L) vacuum vessel, enclosing a volume of 3.1 m^3. The vacuum is achieved through two dry pumps, with a capacity of 80 m^3/h each and two turbo-molecular pumps, with a flow capacity of 2000 l/s each. This setup enables the system to achieve a vacuum pressure of 1.33 × $10^{-}6$ Pa (or $10^{-}8$ Torr)[13].

Over the last section, it has been established how to accomplish toroidal magnetic confinement, creating two magnetic fields: a toroidal field and a poloidal field. In SMART, the toroidal field is produced by a set of twelve Toroidal Field Coils (TFC), each composed of windings with a square cross-section measuring 35 x 35 mm. These windings gradually decrease in size to a 21 x 21 mm cross-section as they extend towards the inboard limbs. On the other hand, the poloidal field is generated by the plasma current, induced by the time-dependent magnetic field from the central solenoid. The central solenoid is a copper coil that is 1.55 meters in height, with an inner

[8] Description of plasma geometry is in the appendix B.

radius of 0.12 meters and an outer radius of 0.15 meters. This solenoid is positioned around the central Toroidal Field Coil (TFC) stack. It is constructed using 240 solid copper windings, each having a square cross-section measuring 11 x 11 mm .

Controlling and shaping the plasma comes from two pairs of axially variable Poloidal Field Coil (PFC) sets, incorporating 23, 11 x 11 mm, windings. The PF1 coils, as shown in figure 5, are located outside the vessel to maximize the plasma volume. The system incorporates two pairs of fixed Divertor (Div) coil sets, allowing for operation in either an upper or lower single-null or a double-null configuration. In a double-null configuration, the plasma is symmetric concerning the Z-axis. Knowing the set of coils comes in pairs, symmetry is achieved by coupling the current in each pair of coils. In single-null configurations, this symmetry is lost, meaning the currents become uncoupled to reach the desired shape. The Div1 set is constructed with a larger 35-winding design, utilizing the same 11 x 11 mm winding cross-section. The Div2 coil set is built similarly to the PFC, also serving as the vertical control feedback coil[13] .

The gas injected in a tokamak must be ionized to become plasma and commence the confinement. This process is referred to as plasma breakdown. The tokamak SMART achieves ionization, utilizing a classic inductive breakdown. The Lloyd criterion for magnetized plasma [14] describes that the minimum electric field E_{bd} required for the breakdown of hydrogen or deuterium gas, given a pressure p (Torr), can be approximated as:

$$E_{bd} = \frac{1.25 \cdot 10^4 p}{\ln(510 p L_c)} , \tag{2.47}$$

where L_c is defined as:

$$L_c = 0.25 a_{eff} \frac{B_\phi}{B_\theta} , \tag{2.48}$$

where a_{eff} is the effective plasma radius. B_ϕ and B_θ are the toroidal and the poloidal coordinates of the vacuum magnetic field, also known as the null-field. Furthermore, one empiric equation is commonly used as metrics to assess and ensure the reliable occurrence of breakdown[13]:

$$E_{bd} \frac{B_\phi}{B_\theta} \geq 1000 \; V m^{-1} . \tag{2.49}$$

From equations 2.47, 2.48 and 2.49 it can be proven, for an operational pressure range, that E_{bd}

is optimized by minimizing the B_θ. A clever configuration of the PF and Div coils can decrease the null-field prior to the solenoid ramp-down. The solenoid initiates the plasma breakdown and the ohmic heating, apart from preserving the plasma current.

When performing experiments in the tokamak SMART, parasitical eddy currents emerge in the vessel. Eddy currents are circulating electrical currents induced in a conductor when it is exposed to a changing magnetic field. They can be explained by applying the already mentioned Maxwell-Faraday's law, 2.46. They create heat, oppose the inducing magnetic field, and depend on factors like the conductor's material and the frequency of the changing field. To reduce the formation of eddy currents, the vessel utilizes a 4 mm thick inboard wall and an 8 mm thick outboard wall with two more substantial upper and lower lids, each measuring 15 mm in thickness, securely bolted to the vessel to facilitate maintenance access.

SMART will be developed through three stages, each representing a substantial enhancement in terms of pulse duration, heating power, and the range of attainable plasma geometries. Phase 1 will mark the initiation of the first plasma, using hydrogen, and will function as a proof-of-concept for device diagnostics and operational procedures. In Phase 2, coupled with an elevation in toroidal field strength and plasma current, Neutral Beam Injection (NBI) heating will be introduced, showcasing the ability to achieve highly shaped negative and positive triangularities within a low aspect ratio hydrogen plasma. Phase 3 signifies a substantial escalation in toroidal field strength, plasma current, and discharge timescale, positioning SMART alongside other cutting-edge current generators [13].

2.2 Magnetohydrodynamics

A key aspect of toroidal magnetic confinement is plasma equilibrium. Multiple forces arise when trying to confine plasma able to destabilize the system. The objective of a tokamak is to contain plasma as long as possible to reach ignition, which requires precise control of all the variables associated with equilibrium. Once the behaviour of charged particles in electromagnetic fields has been explained, it is time to jump to the next level of abstraction and model plasma dynamics considering the whole system. As established before, plasma consists of an ionized gas, i.e., ions and electrons. It also shares characteristics with fluids, bringing to the table the possibility of describing plasma as two interacting fluids of different charged natures. This description of plasma

is known as the two-fluid model. The magnetohydrodynamics -MHD- seeks to elucidate plasma analysis further, as it describes plasma as a single fluid followed by a set of differential equations.

In the context of magnetohydrodynamics, various characteristic scales are crucial. These scales are:

Length scale L: Typically, L is proportional to the plasma parameter a, which represents the characteristic size or radius of the plasma. In the case of a tokamak, this is the minor radius of the torus.

Time scale τ: τ is associated with the collision time and is roughly proportional to $\frac{a}{v_{Ti}}$, where v_{Ti} represents the ion thermal velocity. This scale reflects how long it takes for particles to collide and change their trajectories.

Velocity scale v_{Ti}: The characteristic velocity scale, u_i, is similar to v_{Ti}. This is defined by the thermal velocity of ions in the plasma.

In order to proceed in the analysis, it's necessary to compare these to the scales that naturally appear in the system. This comparison helps decide which terms should be retained and which ones can be neglected in the MHD equations. The first simplification surges when comparing the time scale in MHD with the typical electron frequency inside the tokamak plasma. In terms of frequency, $\omega \sim \frac{1}{\tau} \sim \frac{v_{Ti}}{a}$ is surpassed in many orders of magnitude by the electron frequencies, $\omega << \omega_{ce} \sim \omega_{pe}$ [6], where ω_{ce} is the electron cyclotron frequency and ω_{pe} is the electron plasma frequency, both defined in subsection 2.1.2. This suggest that the electron response is quick enough to approximate its mass to zero, $m_e \to 0$.

The second simplification comes from the non-relativistic scale of the macroscopic plasma flow. Any system consisting of charged particles obey Maxwell equations:

$$\begin{aligned} \nabla \cdot \vec{E} &= \frac{q}{\epsilon_0}\,, \\ \nabla \cdot \vec{B} &= 0 \\ \nabla \times \vec{E} &= -\frac{\partial \vec{B}}{\partial t}\,, \\ \nabla \times \vec{B} &= \mu_0 \left(\vec{j} - \epsilon_0 \frac{\partial \vec{E}}{\partial t} \right)\,. \end{aligned} \tag{2.50}$$

Since $v_{Ti} << c$, by enough orders of magnitudes, the displacement current in Maxwell equations

can be ignored. The third simplification, also affecting Maxwell equations, rises from the length scale comparison. Plasma in tokamaks satisfies the inequality $a >> \lambda_D$, leading to the quasineutrality relation: $n_e \approx n_i$. This hints that Gauss's law can be neglected, implying that $\epsilon \nabla \cdot \vec{E} << e n_e$.

Applying these simplifications to the two-fluid model and also introducing the single-fluid variables into its correspondent equations, it is possible to deduce the MHD model [6]. The single-fluid variables are the mass density ρ, the macroscopic velocity v and the pressure p. Their definitions are as follows. The ions are more massive than electrons, thus the density is defined as:

$$\rho = m_i n \ , \tag{2.51}$$

where $n_e = n_i = n$ because of quasineutrality. Also, since $m_i >> m_e$, the momentum of the fluid is carried by the ions [6]. Therefore, the macroscopic velocity is defined as:

$$\vec{v} = \vec{u}_i \ . \tag{2.52}$$

The electron fluid velocity is defined from the current density and the macroscopic velocity:

$$\vec{j} = en(\vec{u}_i - \vec{u}_e) \ , \qquad \vec{u}_e = \vec{v} - \frac{\vec{j}}{en} \ . \tag{2.53}$$

Lastly, the pressure consists of the sum of the ion and electron individual contributions:

$$p = p_e + p_i \ . \tag{2.54}$$

Gathering the simplifications and single-fluid variables, and introducing them into the two-fluid model leads to the following set of equations [6]:

$$\begin{aligned} \frac{\partial \rho}{\partial t} &= \nabla \cdot (\rho \vec{v}) \ , \qquad \text{[Continuity equation]} \\ \rho \left[\frac{\partial \vec{v}}{\partial t} + (\vec{v} \cdot \nabla)\vec{v} \right] &= \vec{j} \times \vec{B} - \nabla p \ , \qquad \text{[Momentum conservation]} \\ \vec{E} + \vec{v} \times \vec{B} &= \eta \vec{j} \ , \qquad \text{[Ohm's law]} \\ \frac{\partial (p \rho^{-\gamma})}{\partial t} &= -(\vec{v} \cdot \nabla)(p \rho^{-\gamma}) \ , \qquad \text{[Energy conservation]} \end{aligned} \tag{2.55}$$

with the simplified Maxwell equations:

$$\begin{aligned} \nabla \times \vec{E} &= -\frac{\partial \vec{B}}{\partial t} , \quad \text{[Maxwell-Faraday equation]} \\ \nabla \times \vec{B} &= \mu_0 \vec{j} , \quad \text{[Ampere's law]} \\ \nabla \cdot \vec{B} &= 0 , \quad \text{[Gauss's law of magnetism]} \end{aligned} \tag{2.56}$$

where η is the resistivity and γ is the adiabatic index. This model comes with some limitations [15], as it is unable to describe multiple phenomena in fusion plasmas, such as radiation, resonant particle effects, micro instabilities, α particle behavior, etc. However, it can accurately depict how magnetic field geometry affects plasma macroscopic equilibrium and stability of fusion plasma. Let us try to approach plasma equilibrium inside the tokamak with this new set of tools. For

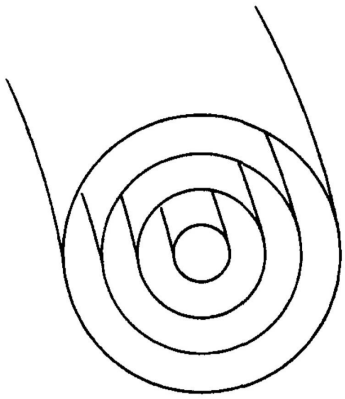

(a) Nested toroidal magnetic surfaces. Source: [5]

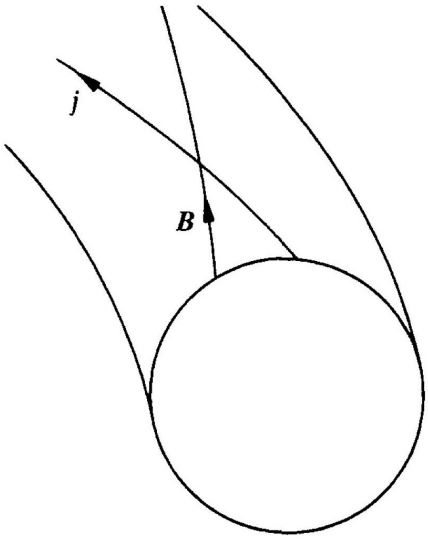

(b) The magnetic field and the current density are contained in the same surfaces. Source:[5]

Figure 6: Poloidal magnetic flux optimized equilibrium.

simplicity, *axisymmetric static* equilibrium will be considered. For axisymmetric equilibrium, i.e., independent from the toroidal angle ϕ, the magnetic field lines distribute in nested toroidal magnetic surfaces[9] as seen in figure 6a. The principal condition for static equilibrium is net zero

[9] This can be proven through Poincaré's theorem, see in [16]

velocity, thus canceling the first term in the momentum conservation equation:

$$\vec{j} \times \vec{B} = \nabla p \ . \tag{2.57}$$

This means that the magnetic force must balance the pressure the plasma exerts. From this equation, it is possible to extract some interesting results. Applying the vector product of $\vec{B}$ and both terms of the equation 2.57, gives the following result, $\vec{B} \cdot \nabla p = 0$. Thus, there is no pressure gradient along the magnetic lines, i.e, the magnetic surfaces have a constant pressure.

Following the same logic as before, the following equation is deduced, $\vec{j} \cdot \nabla p$. Meaning that the current density lines are contained in the magnetic surfaces as shown in figure 6b.

By definition, a toroidal surface densely covered by a magnetic field is called a *flux surface* [16]. It have been discussed how the magnetic field lines, current density and pressure behave on these flux surfaces. In tokamak and stellarator physics is convenient to take advantage of this symmetries and define new functions for the variables that the MHD model works with.

Let us introduce the poloidal magnetic flux function $\Psi(r)$ as:

$$\Psi(r) = \int_{S_p(r)} dS\vec{n} \cdot \vec{B} \tag{2.58}$$

where S_p is a ribbon-like surface, stretched between the magnetic axis and a line of constant θ on the flux surface, labelled by r, with $\vec{n} = \dfrac{\nabla\theta}{|\nabla\theta|}$ as the normal to the surface. On the other hand the toroidal magnetic flux Φ is defined as:

$$\Phi(r) = \int_{S_t(r)} dS\vec{n} \cdot \vec{B} \tag{2.59}$$

where $S_t(r)$ is a disk whose rim joins the flux surface, labelled by r, with $n = \dfrac{\nabla\phi}{|\nabla\phi|}$ as the normal to the surface. A depiction of this surfaces is shown in figure 7. The function of interest will be $\Psi(r)$. This function is determined by the poloidal flux lying within each toroidal flux surface, therefore must be a constant on that surface [5]. This implies that $\vec{B} \cdot \nabla\Psi(r) = 0$.

Taking Gauss's law for magnetism and using the cylindrical coordinates applied to the toroidal

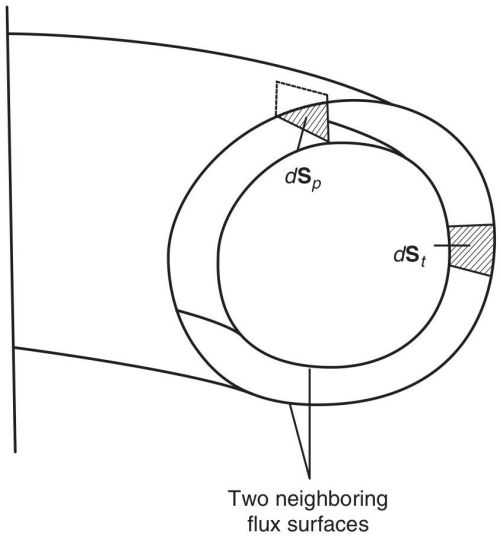

Figure 7: Toroidal and poloidal differential surfaces. Source: [15]

symmetry, $\nabla \cdot \vec{B} = 0$ can be written as:

$$\frac{1}{R}\frac{\partial}{\partial R}(RB_R) + \frac{\partial B_z}{\partial z} = 0 \ . \tag{2.60}$$

It is convenient to introduce a stream function $\psi = RA_\phi$, where A_ϕ is the toroidal component of the vector potential. This function can be related to the poloidal flux function as $\Psi(r) = 2\pi\psi$[10]. This function relates to the poloidal field as:

$$B_R = -\frac{1}{R}\frac{\partial \psi}{\partial z} \ , \quad B_z = \frac{1}{R}\frac{\partial \psi}{\partial R} \ . \tag{2.61}$$

The current density function $\vec{j}$ also lies on the toroidal flux surfaces, meaning that a current flux function also exists. The current flux function f can be related to the poloidal current density as:

$$j_R = -\frac{1}{R}\frac{\partial f}{\partial z} \ , \quad j_z = \frac{1}{R}\frac{\partial f}{\partial R} \ . \tag{2.62}$$

Interestingly, when comparing 2.62 with Ampere's equation:

$$j_R = -\frac{1}{\mu_0}\frac{\partial B_\phi}{\partial z} \ , \quad j_z = \frac{1}{\mu_0}\frac{1}{R}\frac{\partial f}{\partial R}(RB_\phi) \ , \tag{2.63}$$

[10] For a more in depth analysis, consult [15].

it is found that

$$f = \frac{RB_\phi}{\mu_0} \,. \tag{2.64}$$

It can be proven that f is a function of ψ by taking the scalar product of equation 2.57 with $\vec{j}$, which results in $\vec{j} \cdot \nabla p = 0$. Using the result form equation 2.62 and introducing into the last result gives:

$$\frac{\partial f}{\partial R}\frac{\partial p}{\partial z} - \frac{\partial f}{\partial z}\frac{\partial p}{\partial R} = 0 \,. \tag{2.65}$$

Consequently:

$$\nabla f \times \nabla p = 0 \,, \tag{2.66}$$

meaning that f is a function of p. Then, since the pressure is also a function of ψ[11], f is also a function of ψ, $f = f(\psi)$.

2.2.1 Grad-Shafranov equation

In an axisymmetric system like a tokamak, the equilibrium equation can be expressed as a differential equation for the poloidal flux function per radian unit ψ[12]. Equation 2.57 con be rewritten as:

$$\vec{j_p} \times \vec{i_\phi} B_\phi + j_\phi \vec{i_\phi} \times \vec{B_p} = \nabla p \,, \tag{2.67}$$

where $\vec{j_p}$ is the poloidal current density, $\vec{B_p}$ is the poloidal magnetic field and $\vec{i_\phi}$ is the unit vector in the ϕ direction. The equations 2.61 and 2.62 that define the poloidal magnetic field and poloidal density current can be compacted to:

$$\vec{B_p} = \frac{1}{R}(\nabla\psi \times \vec{i_\phi}) \tag{2.68}$$

and

$$\vec{j_p} = \frac{1}{R}(\nabla f \times \vec{i_\phi}) \,. \tag{2.69}$$

[11] Magnetic surfaces are also pressure surfaces, as shown in figure 6b.
[12] As established before, $\Psi = 2\pi\psi$.

Substituting equations 2.68 and 2.69 into the equation 2.67, and using the fact that $\vec{i_\phi} \cdot \nabla\psi = \vec{i_\phi} \cdot \nabla f = 0$ results in:

$$-\frac{B_\phi}{R}\nabla f + \frac{j_\phi}{R}\nabla\psi = \nabla p \; . \tag{2.70}$$

Calculating both gradients for f and ψ:

$$\nabla f(\psi) = \frac{df}{d\psi}\nabla\psi \; , \qquad \nabla p(\psi) = \frac{dp}{d\psi}\nabla\psi \; , \tag{2.71}$$

and introducing them into the equation 2.70 gives:

$$j_\phi = R\frac{dp}{d\psi} + B_\phi\frac{df}{d\psi} \; . \tag{2.72}$$

Now, using equation 2.64 to substitute B_ϕ into equation 2.72 results in:

$$j_\phi = Rp' + \frac{\mu_0}{R} f f' \; , \tag{2.73}$$

where the derivative with respect to ψ is written with an apostrophe. To express j_ϕ in terms of ψ, Ampere's law is applied:

$$\mu_0\vec{j} = \nabla \times \vec{B} \; . \tag{2.74}$$

Substituting equations 2.62 into the toroidal component of equation 2.74 gives:

$$-\mu_0 R j_\phi = R\frac{\partial}{\partial R}\frac{1}{R}\frac{\partial\psi}{\partial R} + \frac{\partial^2\psi}{\partial z^2} \; . \tag{2.75}$$

Finally, using equation 2.75 to substitute for j_ϕ in equation 2.73 results in the desired differential equation:

$$R\frac{\partial}{\partial R}\frac{1}{R}\frac{\partial\psi}{\partial R} + \frac{\partial^2\psi}{\partial z^2} = -\mu_0 R^2 p'(\psi) - \mu_0^2 f(\psi) f'(\psi) \; . \tag{2.76}$$

The resulting equation is known as *Grad-Shafranov equation.*

2.3 Plasma resistivity

In the face of an electrical field, electrons would accelerate indefinitely along the magnetic field lines. However, collision events between electrons and ions will resist this motion, limiting the

current that could be driven by the applied voltage, giving rise to electrical resistivity η. As a first approach, resistivity may be expressed in terms of the electron-ion collision frequency. In plasma, charged particle collisions come in two main types: collisions with other charged particles and collisions with neutral atoms and molecules. Plasma physicists typically find collisions with other charged particles more intriguing, as they prevail in high-temperature plasma with high-ionization levels. This can be proven by doing a rough estimate on neutral and Coulomb collisions. The cross section for scattering of an electron by a neutral atom may be approximated very roughly as:

$$\sigma_n \sim \pi a_0^2 \sim 10^{-20} m^2 \ . \tag{2.77}$$

where a_0 is the distance which an electron would have a considerable chance of experiencing a large-scale collision. Alternatively, as established in subsection 2.1.2, an electron will loose most of its initial momentum, colliding with an ion, when its energy is comparable to the Coulomb potential, i.e.:

$$\frac{e^2}{4\pi\epsilon_0 b} \sim \frac{mv^2}{2} \sim T_e \ , \tag{2.78}$$

where b is the impact parameter and T_e is the electron temperature, given in eV. The effective Coulomb cross section of the ion would be:

$$\sigma_i \sim \pi b^2 \sim \frac{\pi e^4}{(4\pi\epsilon_0)^2 T_e^2} \sim \frac{10^{-17}}{T_e^2} m^2 \ . \tag{2.79}$$

Later in this subsection, it will be explored the fact that, in reality, the effective Coulomb cross section is almost two orders of magnitude larger due to the cumulative effect of small deflections. Comparing both collisional processes, using equations 2.78 and 2.79 and using the electron temperature to estimate the degree of ionization, it can be proven that, Coulomb collisions will dominate over collisions with neutrals in any plasma that is even just a few per cent ionized [17]. In a tokamak plasma, it is possible to consider that ionization is total, making Coulomb interaction the dominant source of collisions.

2.3.1 Spitzer resistivity

As shown in equation 2.26, the presence of an electric field exerts a force on electrons, accelerating them in the parallel direction. This motion would be opposed by collisions with the non-accelerated particles, specially ions. This is because ions, given their much greater mass, exhibit relatively low responsiveness to the applied electric field. Therefore, the Coulomb force will be balanced by the collisions with ions:

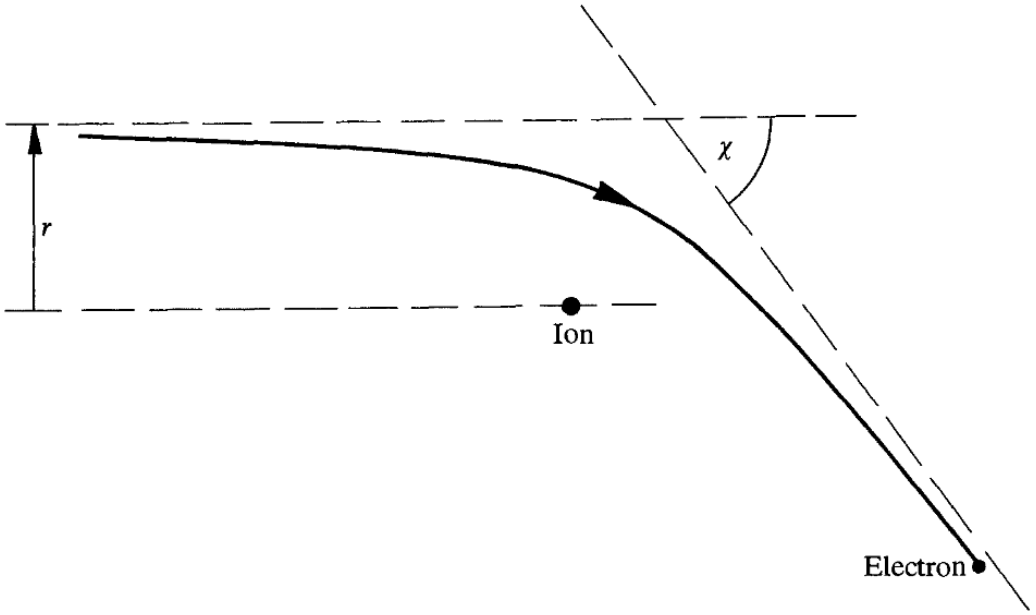

Figure 8: Scattering event between an ion and a electron. Source: [5]

$$Ee = \frac{m_e v_d}{\tau_e} \,, \tag{2.80}$$

where v_d is the equilibrium velocity of the electrons and τ_e is the electron collision time. Calculating this collision time can be quite complex. Firstly, the concept of collision in a plasma is nuanced. Secondly, these collisions are contingent on the relative velocities of the particles involved, and the net outcome results from the collective impact of interactions between particles with varying velocities. On the other hand, the electrical field is not as simple as previously described, it must be decomposed into two main contributions. Let us analyze it from the perspective of a single particle. The first is the uniform macroscopic external field, which accelerates the subject particle. The second is the rapidly fluctuating microscopic electric field, which arises from the presence of the particles that lie inside a Debye sphere surrounding the given particles, damping the other

collisions from remote particles. To simplify the analysis, it will be only considered one to one interactions, and only collisions inside this Debye sphere:

Following Rutherford's scattering theory, the scattering angle χ for an impact parameter r and an incident velocity v, depicted in figure 8, is given by:

$$cot(\chi/2) = \frac{4\pi\epsilon_0 m_e v^2 r}{e^2} \ . \tag{2.81}$$

Using equation 2.81, it is possible to deduce the impact parameter for 90° scatter:

$$r_0 = \frac{e^2}{4\pi\epsilon_0 m_e v^2} \ . \tag{2.82}$$

Thus, the cross section for a scattering of an angle > 90° is:

$$\sigma_0 = \frac{e^4}{64\pi\epsilon_0 E^2} \ , \tag{2.83}$$

where E is the kinetic energy of the electron. Nonetheless, it must be taken into account the cumulative effect of small deflections when considering the loss of momentum and energy of a scattered a particle. Each collision with a single ion leads to the following parallel momentum loss:

$$\delta p = -\frac{2m_e v}{1 + (r/r_0)^2} \ . \tag{2.84}$$

Multiplying 2.84 with the rate of collisions per unit area, i.e. , nv, where n is the ion density and v the electron velocity and integrating over the impact parameter r gives us the total rate of change of momentum:

$$\frac{dp}{dt} = -2nvm_e v^2 \int_0^{\lambda_D} \frac{2\pi r}{1 + (r/r_0)^2} = -2nm_e v^2 \sigma_0^2 ln(1 + (r/r_0))|_0^{\lambda_D} \ , \tag{2.85}$$

where it was used λ_D as the upper limit to neglect the shielded interactions with distant ions. Since $\lambda_D >> r_0$ [5], equation 2.85 transforms into:

$$\frac{dp}{dt} = -4 \ln \Lambda \sigma_0 n m_e v^2 \ , \tag{2.86}$$

where $\ln\Lambda = \ln(\lambda_D/r_0)$ is called the Coulomb logarithm[13]. As a result, proof of the importance of the cumulative effect of small deflections with a greater effective Coulomb cross section $4\ln\Lambda\sigma_0$ is given.

Returning to equation 2.80, when compared to Ohm's law:

$$E = \eta j \ , \tag{2.87}$$

it is possible to find that

$$\eta = \frac{m_e}{n_e e^2 \tau_e} \ , \tag{2.88}$$

for a current density $j = n_e v_d$. To give an accurate vale for the plasma resistivity, it is necessary to compute the electron collision time solving the collisional kinetic electron equation -the Fokker-Planck equation- for the electron distribution function considering also the electron-electron collisions. Spitzer and his co-workers computed the following result [5]:

$$\eta_S = 0.51 \frac{m_e^{1/2} e^2 \ln\Lambda}{3\epsilon_0^2 (2\pi T_e)^{3/2}} = 1.65 \cdot 10^{-9} \frac{\ln\Lambda}{T_e^{3/2}} \Omega \, m \ , \tag{2.89}$$

where T_e is given in keV. Equation 2.89 can be used in absence of a magnetic field or for the current parallel to the magnetic field. In directions perpendicular to the magnetic field, the cyclotron motion of electrons tends to make the electron distribution more isotropic. As a result, the resulting perpendicular resistivity is affected in the following way [5]:

$$\eta_\perp = 1.97 \eta_\parallel \ . \tag{2.90}$$

If the plasma is composed of several ion species, the effective ion charge Z_{eff}[14] must be taken into account, which results in:

$$\eta = Z_{eff} \eta_S \tag{2.91}$$

An interesting result from the Spitzer resistivity model is that the resistivity is reduced when the plasma electron temperature increases.

[13] Consult [5] for a method to compute this logarithm.
[14] See [5] for a computing method.

2.3.2 Neoclassical resistivity

Throughout the analysis of plasma resistivity, plasma has been treated as a homogeneous volume of charged particles, ignoring its geometry inside a tokamak. As seen in subsection 2.1.3, the toroidal geometry comes with different drifts, affecting particle trajectories and, consequently, impacting the description of plasma resistivity. Neoclassical theory tries to depict this phenomenon, including the plasma geometry configuration as a consideration. The transport is still governed by Coulomb collisions.

Neoclassical effects can result in a nearly one order of magnitude increase in plasma resistivity. This can be understood as follows. In a cylindrical system, particles are confined within a gyro radius of a flux surface. Consequently, the step size associated with Coulomb collisions is also roughly the size of a gyro radius. However, in a toroidal system, particles drift away from the flux surface due to toroidally induced $\nabla \boldsymbol{B}$ and curvature drifts. The radial excursions caused by these drifts can be much larger than a gyro radius, leading to an increase in the collisional step size and, consequently, an increase in the resistivity coefficient. Additionally, the resistance resulting from the small number of trapped particles dominates over the one from passing (untrapped) particles [6].

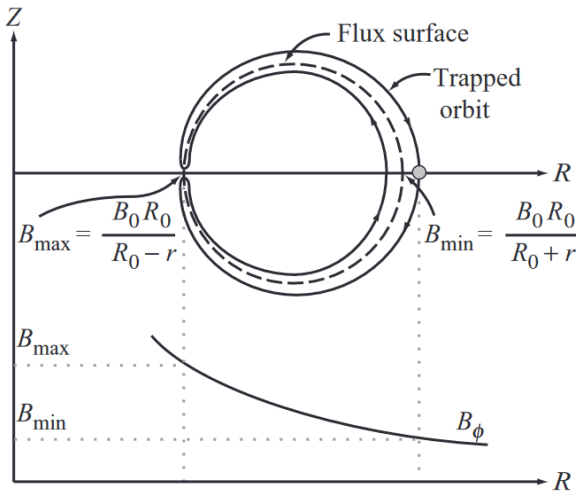

Figure 9: Geometry of a trapped particle orbit between the gradient of the toroidal magnetic field. Source:[6].

Trapped particles exist in a tokamak plasma because of the variation in magnetic field strength within the torus. In a tokamak, the magnetic field is weaker on the outside of the torus and more powerful on the inside, approximately following $\boldsymbol{B} \sim \boldsymbol{B}_\phi \sim \boldsymbol{B}_0(\boldsymbol{R}_0/\boldsymbol{R})$ where $\boldsymbol{R}_0$ is the major radius, $\boldsymbol{R}$ is the radial position, and $\boldsymbol{B}_0$ is the central magnetic field strength. Due to this configuration, particles starting on the outside region of the torus with a small ratio of parallel velocity $v_\parallel$ to perpendicular velocity $v_\perp$ experience mirror reflection. As mentioned in subsection

2.1.3, particles experience a force proportional to a parallel gradient of the magnetic field, shown in equation 2.38

As their parallel motion takes them toward the inside of the torus, where the magnetic field is more intense, these particles become ”trapped” on the outer side of the torus. Trapped particle transport dominates Coulomb transport for several reasons. One significant factor is that trapped particles have relatively small parallel velocities. Consequently, it takes them longer to complete one complete cycle of mirror motion compared to typical passing particles, which finalize one full transit around the poloidal cross-section more rapidly. This lengthier mirror period for trapped particles results in more time to drift away from flux surfaces due to $\nabla \boldsymbol{B}$ and curvature drift, resulting in larger step sizes during collisions. Also, collisions become more frequent for trapped particles as they encounter more obstacles during their trapped orbits.

The overall effect is that the current is reduced by the presence of trapped particles, which are unable to move freely along the magnetic field lines in response to the application of an electric field. The number of trapped particles is directly related with the aspect ratio of the plasma.

One result that supports the neoclassical theory is the prediction of the bootstrap current[6]. The bootstrap current emerges, augmenting the toroidal current, as the plasma diffuses outward. In a tokamak, the pressure gradient applies a radially outward force onto the particles. Recalling the particle drift equation for a generalized force 2.31, the presence of the poloidal magnetic field induced by the plasma current and the internal plasma pressure, produces a drift in the toroidal direction. Figure 10 presents a graphical description of this effect.

It’s as if the tokamak is effectively raising itself ”by its own bootstraps.” [7] Both experimental measurements and theoretical predictions regarding the neoclassical bootstrap current are in good alignment, which is a positive outcome. This alignment is currently considered a critical element in the pursuit of developing an economically viable tokamak reactor. However, it’s just one component of the overall current in the plasma, and other sources of current, such as external heating and current drive methods, are often necessary to achieve the conditions required for sustained nuclear fusion.

Multiple neoclassical resistivity functions have been developed by the scientific community, which consider the influence of trapped particles. As shown in this article [18], one approach to

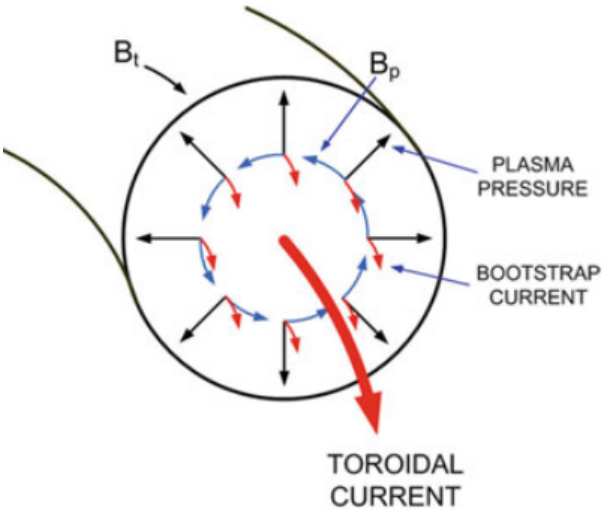

Figure 10: Bootstrap current originating from the particle drift due to the plasma pressure and the poloidal magnetic field. Source: [7]

neoclassical resistivity goes as follows:

$$\eta = \eta_S \frac{Z_{eff}}{(1-\phi)(1-C\phi)} \frac{1+0.27(Z_{eff}-1)}{1+0.47(Z_{eff}-1)}\,, \tag{2.92}$$

where

$$\begin{aligned} \phi &= \frac{f_T}{1+(0.58+0.20Z_{eff})\nu_{*e}}\,, \\ C &= \frac{0.56}{Z_{eff}\dfrac{3.0-Z_{eff}}{3.0+Z_e ff}}\,, \\ \nu_{*e} &= \epsilon^{3/2}\frac{Rq}{v_{Te}\tau_e} \end{aligned} \tag{2.93}$$

R is the major radius of the plasma, q is the safety factor, ϵ^{-1} is the aspect ratio R/a, $v_{Te} = (T_e/m_e)^{1/2}$ and η_S is the Spitzer resistivity coefficient. f_T is the fraction of electrons trapped that, for $\nu_{*e} \to 0$ is:

$$f_T = 1 - \frac{(1-\epsilon)^2}{(1-\epsilon^2)^{1/2}(1+1.46\epsilon^{1/2})} \tag{2.94}$$

and

$$\tau_e = 3(2\pi^{3/2})\frac{\epsilon_0^2 m_e^{1/2} T_e^{3/2}}{n_e e^4 \ln\Lambda} \tag{2.95}$$

is the electron collision time. Z_{eff} is the effective ion charge.

3 Methodology

During this bachelor's thesis, the dynamics plasma equilibrium inside a tokamak device has been explored. To investigate this kind of plasma confinement, it has been made use of FIESTA, a potent numerical framework capable of solving the Grad-Shafranov differential equation and present a solution for the equilibrium flux functions along with other results, such as the current waveforms of the solenoid and control coils, the eddy currents in the vessel or the stress the vessels suffers because of the eddy currents. A key factor of this project was comprehending how FIESTA performs these simulations and learning how to execute them. First, let us give an overview of the numerical methods FIESTA implements.

3.1 FIESTA

Recalling equation 2.57, in an equilibrium state, plasma balances the inward current-induced force $\vec{j} \times \vec{B}$ with the outward thermal pressure p. For a toroidal geometry, this equilibrium can be numerically solved as a solution to the Grad-Shafranov (GS) equation, explored in subsection 2.2.1. A solution for this equation would describe the toroidal plasma current and the toroidal magnetic field. However, this is not the total magnetic field the plasma is subject to. The ultimate equilibrium field results from a combination of factors, including the vacuum magnetic field, which is influenced by the coil's geometry and current configuration, the self-induced magnetic field generated by the plasma, and supplementary fields that emerge from eddy currents within the vessel structure. To create a dependable model of plasma equilibria, it's crucial to understand the geometric and magnetic structure and have access to the time-resolved data on coil currents and plasma currents. Additionally, when addressing plasma breakdown, it's essential to model the eddy currents induced during solenoid and coil ramps before the discharge. These eddy currents influence the null-field (i.e., vacuum) magnetic structure and the criteria for the breakdown [13].

FIESTA was designed to be a code environment with access to different numerical models able to give insight into the plasma equilibria, vacuum field, breakdown and plasma current. To initiate the simulations, the user is presented with a list of required input variables. These are: the vessel geometry, the coil geometry, the coil waveforms (these include the solenoid, poloidal field coils and divertor field coils), the discharge parameters (for these simulations, the specific Phase

1 parameters are used) and the plasma shaping parameters.

The simulations are executed on a 2D rectilinear grid of 300×251 ($R \times Z$) cells, providing a radial resolution of 5 mm per cell and an axial resolution of 2.6 mm per cell. The vessel walls, PF and Div coils and the central solenoid are emulated as toroidal current wires. Table 1a displays the discharge parameters used for Phase 1 simulations. Table 1b shows the plasma shaping parameters which will determine the required poloidal and divertor currents. Once all of these variables are declared, the first program called by FIESTA is TOPEOL.

FIESTA discharge parameters		
Electron temperature	T_e	120 eV
Ion temperature	T_i	95 eV
Toroidal magnetic field	B_t	0.1 T
Plasma current	I_p	100 kA
Effective ion charge	Z_{eff}	$2{\cdot}1.6 \cdot 10^{-19}$ C
Electron density	n_e	$1.08{\cdot}10^{19}$ m^{-3}

(a)

Shaping parameters of the plasma	
Radial centre position	R_{geo}
Aspect ratio	A
Elongation	κ
Triangularity	δ
Axis centre position	Z_{geo}

(b)

Table 1: T_e, T_i, n_e are given by ASTRA [13]

TOPEOL, using a linear model, obtains a precomputed plasma density profile J(R) at a time τ, evaluated from the poloidal β_θ, defined as:

$$\beta_\theta = 3\mu_0 e n_e \kappa \frac{(T_e + T_i)}{\mu_0 I_p / 2\pi a} \tag{3.1}$$

where the parameters present in the equation are obtained from the user input. They are all referred in tables 1a and 1b. To deduce the J(R), first p' and ff' are scaled relative to β_θ via equations 3.2 and 3.3 [12]:

$$p' = \frac{\beta_\theta (1 - \psi_n)}{R_{geo}} , \tag{3.2}$$

$$f f' = \mu_0 R_{geo} (1 - \beta_\theta)(1 - \psi_n) , \tag{3.3}$$

where ψ_n is the normalised poloidal flux, defined as: $\psi_n = \dfrac{\psi - \psi_0}{\psi_b - \psi_0}$. ψ_0 is the poloidal flux on the axis at R_{geo}, and ψ_b is the poloidal flux at the last closed surface boundary. Thus, the J(R) is computed through this estimations. Then, the output is transferred to the EFIT program, which solves the Grad-Shafranov equation and returns a first iteration of an optimised equilibrium $\psi(R, Z)$

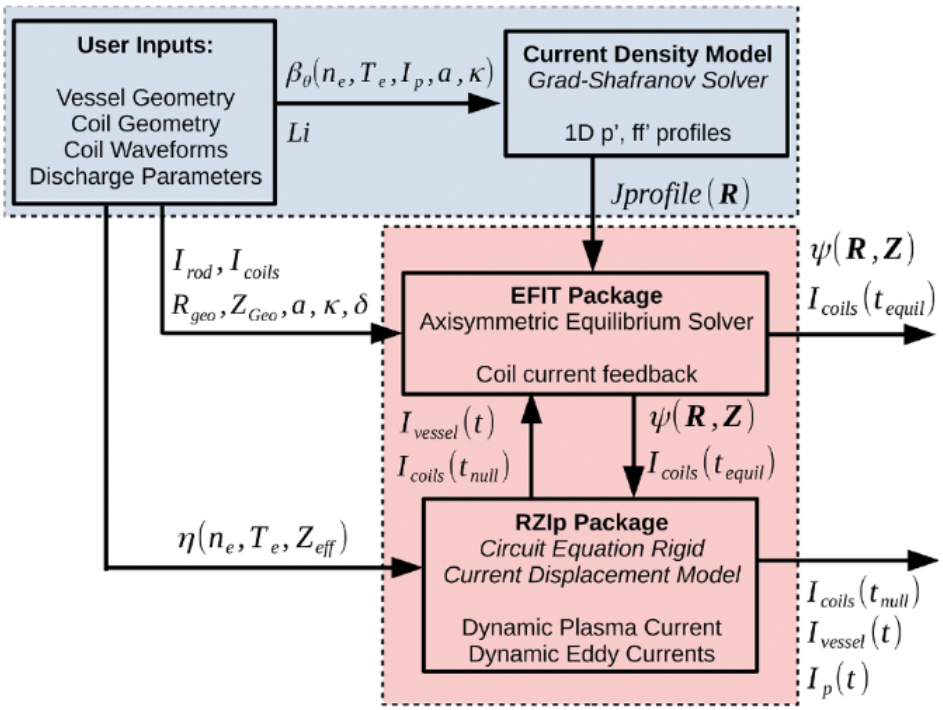

Figure 11: FIESTA flux diagram. Source: [13].

given the objective shaping parameters and the coil current boundary conditions. Next, EFIT sends this simulation to the RZip code.

RZip computes the time-resolved vessel, coil and plasma current evolution, through the employment of the following matrix system[13]:

$$\mathcal{M}\frac{d\mathbf{I}}{dt} + \mathcal{R}\mathbf{I} = \mathbf{V}\ , \tag{3.4}$$

where $\mathcal{M}$ is a symmetric square matrix whose diagonals elements contain the self-inductance of the coil and vessel filaments, and whose triangular elements contain the mutual coil-to-coil, vessel-to-vessel and coil-to-vessel inductance, $\mathcal{R}$ is a diagonal matrix containing the resistance of each filament and $\mathbf{I}$ and $\mathbf{V}$ are vectors of the dynamics currents and voltages of the filaments.

The simulated results are then sent back to EFIT, giving feedback to the first equilibrium found and adjusting it to comply with the new total magnetic field. An overview of this process is represented in figure 11.

When trying to compute FIESTA simulations is key to understand how the PF, Div coils and eddy-currents affect the plasma equilibrium. During this research, it was found that the best

way to predict how the simulation will evolve and achieve equilibria is to consider the plasma as a current density that feels a force originating from the currents on the control coils. Let us picture this idea using two linear current densities as a simplified model. As shown in figure 12, any current density will create a magnetic field, following Ampere's law. This magnetic field

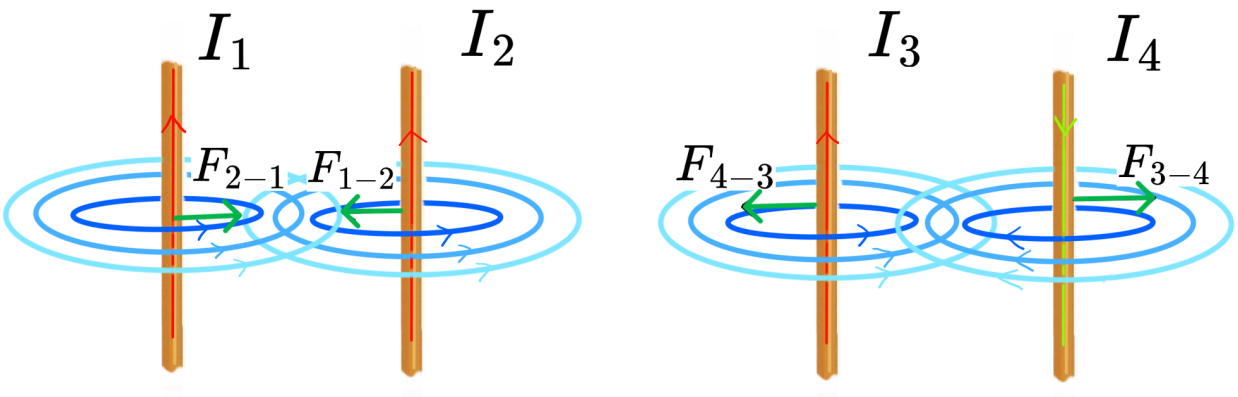

Figure 12: Two facing currents exerting a force to each other.

will apply a force on a neighbouring current. Consequently, this neighbouring current will also exert, on the first current, a force relative to the current directions. It is possible to extend this idea to plasma. Considering a section of the plasma current density, it can be described as an array of linear density currents. If another linear density current is nearby, it will exert a force -decreasing with distance- on the linear current densities that define the totality of the plasma. In figure 13 a depiction of this idea is shown. This way, trying to give an intelligent guess on the

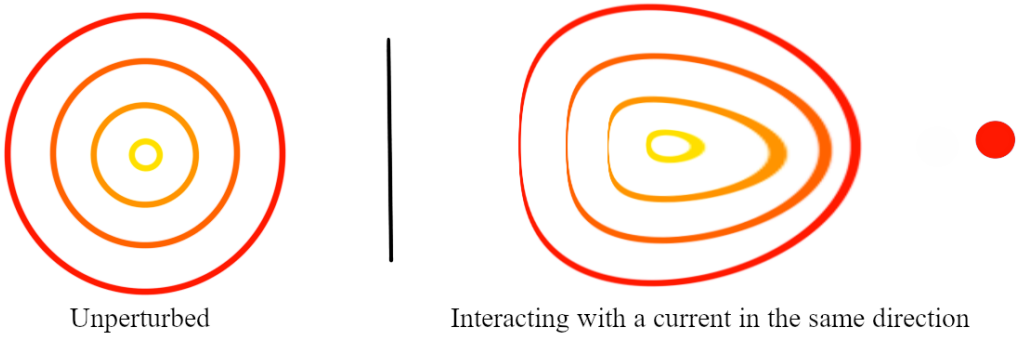

Figure 13: Plasma deformation because of the poloidal control currents.

initial conditions for the current waveform becomes easier, taking into account the target shape.

4 Results

Firstly, when does FIESTA takes the *plasma resistivity* into account?

As described in last section, RZip is on charge of computing the plasma current waveform, so it requires the plasma resistivity as a parameter. During the simulations, FIESTA calls a function dedicated exclusively to compute the plasma resistivity as a function of the plasma discharge parameters. Originally, this function was based on the Spitzer resistivity model, making use of the equation 2.89. As part of this bachelor's thesis a decision branch was implemented for the user interface, that enables the option between the two resistivity models and a new function that considers the neoclassical resistivity equations, presented in subsection 2.3.2. On one hand,

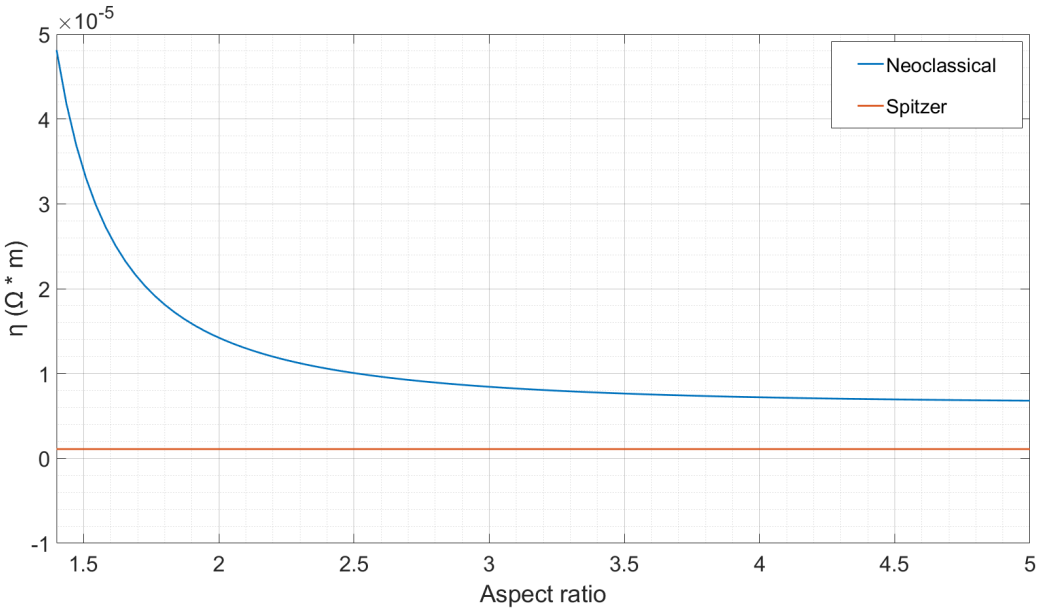

Figure 14: Comparison between the neoclassical resistivity model and the Spitzer model against the plasma aspect ratio. The discharge parameters are constant and correspond to those appearing in table 1a. Computed with Matlab using the functions implemented in FIESTA.

the Spitzer resistivity model only depends on the plasma discharge parameters, which troughout the simulations are considered constant. On the other hand, the neoclassical resistivity model depends on the number of trapped particles within the plasma, which depends directly on the aspect ratio. Figure 14 shows how the resistivity evolves against the aspect ratio.

A first interesting result arising from the consideration of trapped particles is, that for an aspect ratio < 2.5, the neoclassical resistivity is an order of magnitude greater than the Spitzer

approach, already suggesting the importance of considering the plasma geometry.

When interpreting figure 14 it must be considered the fact that, the tokamak SMART, as its name indicates, works in the range of A$\in$ (1.6, 2.0). Thus, in practicality, plasmas resistivity will be always one order of magnitude grater than the Spitzer prediction.

The increase of the resistivity will impact mainly on the induced plasma current, required to create the poloidal magnetic field that confines the tokamak plasma. Let us compare two plasma simulations, with similar target shaping parameters but each with a different resistivity model.

4.1 FIESTA simulations. Spitzer vs. Neoclassical

Every simulation performed in the FIESTA code environment comes with numerical data and graphical representations of relevant aspects of the SMART plasma dynamics along the duration of the pulse discharge. It was found that, from all this data, the most significant results about the change in the plasma resistivity were the equilibrium poloidal flux functions, the eddy currents, the coil current waveform and the plasma current.

In the tables 2a and 2b, the target shape parameters and optimized output given by FIESTA are registered. Even though the discharge and the objective shape parameters are equal for both simulations, FIESTA finds different equilibrium solutions. Besides, the iterated geometry parameters differ somewhat from the desired plasma shape. This is expected, given that the final equilibrium is influenced by the initial guess for the PF and Div coil currents, the emerging eddy currents and, consequently, the plasma resistivity.

Spitzer resistivity			
Rgeo	0.46	Rgeo_{efit}	0.45997
A	1.85	A_{efit}	1.8850
κ	1.6	κ_{efit}	1.6491
δ	0.4	δ_{efit}	0.39489
Zgeo	0.0	Zgeo_{efit}	0.0000

(a)

Neoclassical resistivity			
Rgeo	0.46	Rgeo_{efit}	0.45980
A	1.85	A_{efit}	1.9111
κ	1.6	κ_{efit}	1.5867
δ	0.4	δ_{efit}	0.4604
Zgeo	0.0	Zgeo_{efit}	0.0000

(b)

Table 2: Target shaping parameters and the optimised values by EFIT for each resistivity model

Looking at the figures 15a and 15b, at first glance, the overall geometry of the plasma is consistent for different resistivity models. Nevertheless, the poloidal magnetic flux for the neoclassical approach is one order of magnitude greater than the Spitzer model. Recalling equation 2.59,

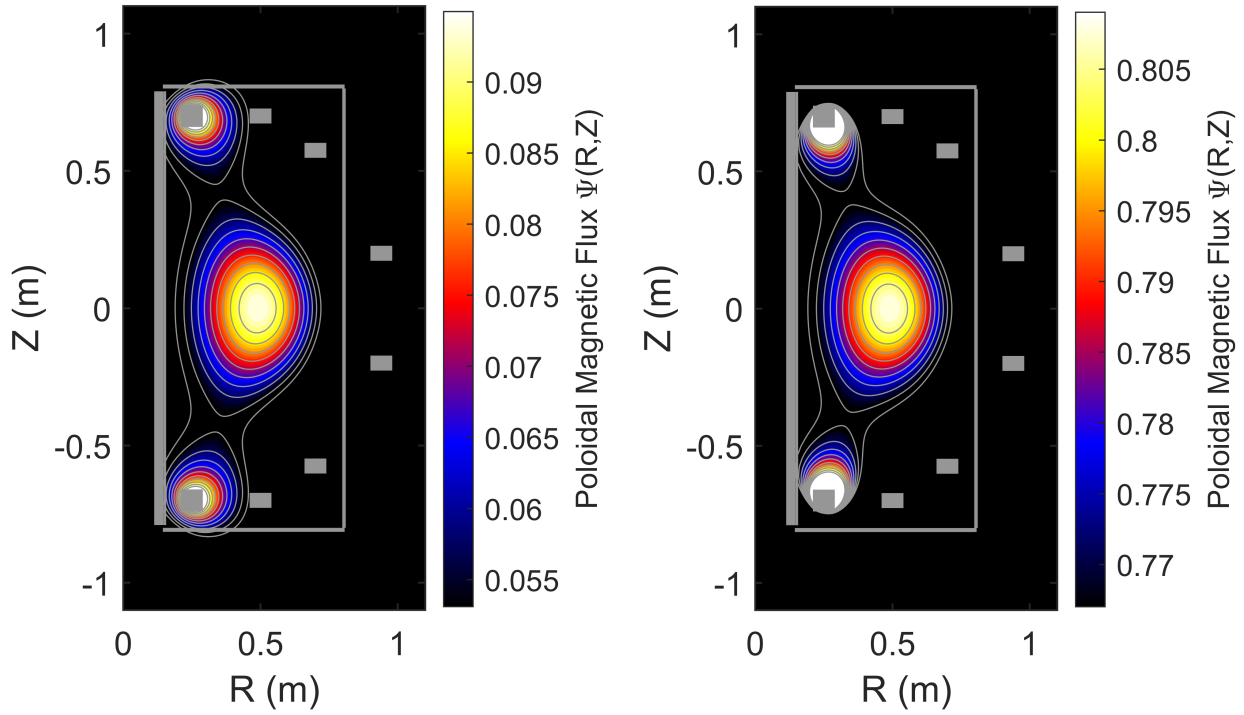

(a) Spitzer resistivity

(b) Neoclassical resistivity.

Figure 15: Poloidal magnetic flux optimized equilibrium.

the poloidal magnetic flux $\psi(R, Z)$ is a function of the poloidal magnetic field. Therefore, this variation must originate from the sources of poloidal magnetic field in the tokamak SMART.

The toroidal magnetic confinement relies on the self-induced plasma poloidal field generated by the plasma current. Given that both simulations achieve a plasma current of 100 kA, the difference in poloidal fluxes rises from other phenomena. The already mentioned plasma current is induced by varying central solenoid current, which generates a time-dependent magnetic field that, as Maxwell-Faraday's law indicates,

$$\nabla \times \vec{E} = -\frac{\partial \vec{B}}{\partial t} \,, \tag{4.1}$$

induces an electrical field inside the tokamak plasma. Following Ohm's law:

$$E = \eta j \,, \tag{4.2}$$

the required electric field to achieve the desired plasma current is directly proportional to the

resistivity. Combining equations 4.1 and 4.2, indicates that a greater resistivity implies a greater solenoid magnetic field, and consequently a more intense current. This will be reflected in the solenoid current waveform.

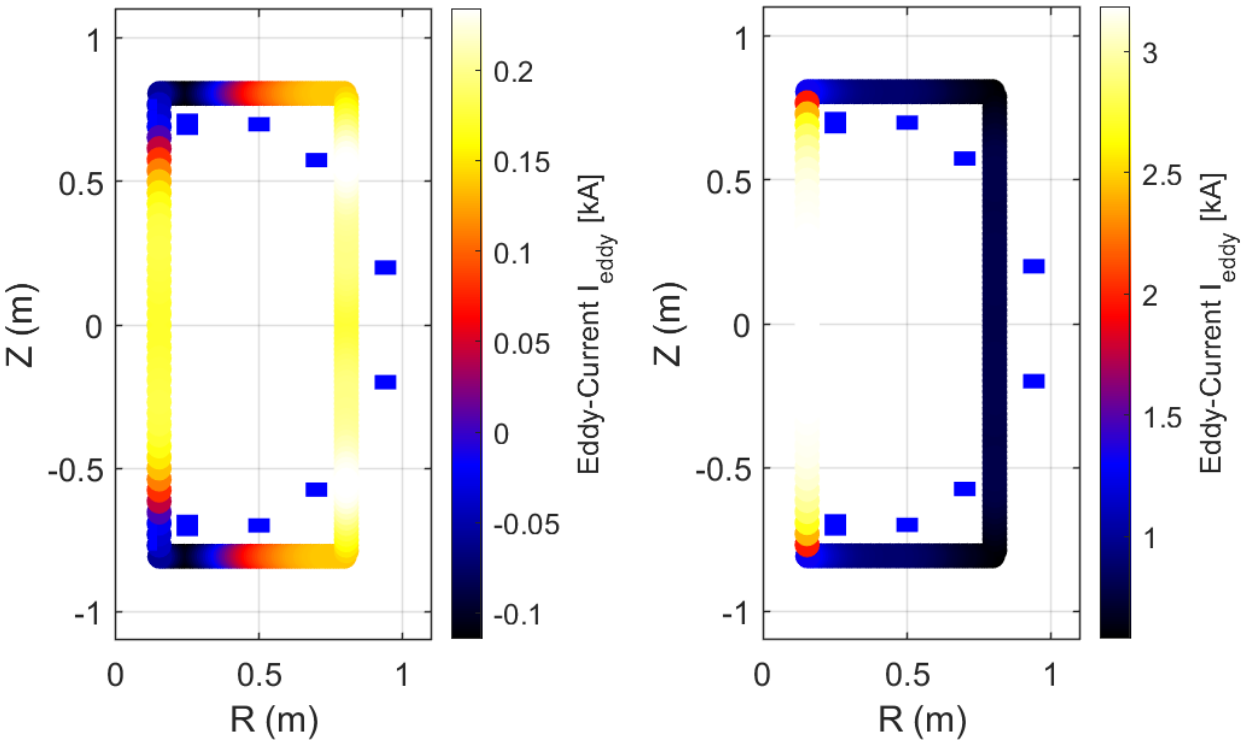

(a) Spitzer resistivity

(b) Neoclassical resistivity.

Figure 16: Eddy currents resulting from the presence of magnetic fields.

Next, the influence of the eddy currents as one of the reasons for differing magnetic poloidal fluxes is explored. On one hand, figure 16a reveals that, for the Spitzer resistivity model, the eddy-currents are approximately evenly distributed along the SMART vessel, and appear mainly because of the PF coils and the solenoid [15]. On the other hand, figure 16b shows that, for the neoclassical resistivity model, the eddy currents, although present along the whole vessel, are severely intense on the inner wall where the solenoid is located. Again, this reveals the impact the solenoid current suffers when considering the trapped particles inside the tokamak plasma. Apart from the inhomogeneous distribution of eddy currents, these are one order of magnitude greater in the newly implemented model. In subsection 3.1, a qualitative description of how the control coil currents deformed the tokamak plasma was given. The eddy currents act on plasma

[15] See figure 5 for a reference on coils' names

dynamics analogously. Usually, parasitical eddy current currents must be counteracted with the PF and Div coils, which translates into the requirement of stronger coil currents -compared with the ideal case of nonexistent eddy currents-. As one can expect, the eddy currents contribute in the more intense poloidal flux function.

It has been already mentioned a couple of times the impact the resistivity model has on the solenoid current, thus the next topic will be the numerical results of the solenoid current given by the FIESTA simulations. There are four significant time periods considered in the SMART plasma computations.

·**Null-field period** (from -20 ms to 0 ms): Determines the null-field decay timescale.

·**Breakdown Ramp period** (from 0 ms to 4 ms): Determines the maximum loop voltage.

·**PF & Div Ramp period** (from 4ms to 15 ms): Determines maximum PF & Div current ramp.

·**Pulse period** (from 15 ms to 115ms): Determines the flat-top timescale.

For theses timescales, the user declares adequate solenoid current ramps, which enable the target plasma current. Unlike the solenoid current, which is exclusively modified by the user, the control coil currents are optimised by FIESTA. The user inputs solely an initial guess for the equilibrium coil currents. Figures 17 and 18 depict the current waveforms along all the previously mentioned time stamps. Clearly, the most significant impact that the neoclassical resistivity model has in the tokamak SMART plasma equilibrium is on the solenoid current waveform. For the neoclassical model, the solenoid current encompasses values starting from 85.5 kA to -85.5 kA, unlike the Spitzer model predictions with a more moderate intensity, with a maximum of 6.5 kA and a minimum of -6.5 kA. The control coils also suffer an increase in intensity, rising from the previously mentioned stronger eddy currents. Precisely, the PF and Div coils are meant to modify the poloidal magnetic field in order to shape and stabilize the plasma, influencing the poloidal flux function. This control coil's current increment becomes another contributor to the intensified poloidal flux in the neoclassical model.

Solenoid waveform				
Time period τ (ms)	(-20, 0)	(0, 4)	(4, 15)	(15, 115)
I_{sol} (kA)	(6.5, 6.5)	(6.5, 4.0)	(4.0, 3.0)	(3.0, -6.5)
dI/dt (kA/ms)	0	0.625	0.0667	9.5

Table 3: Input solenoid current, using the Spitzer model.

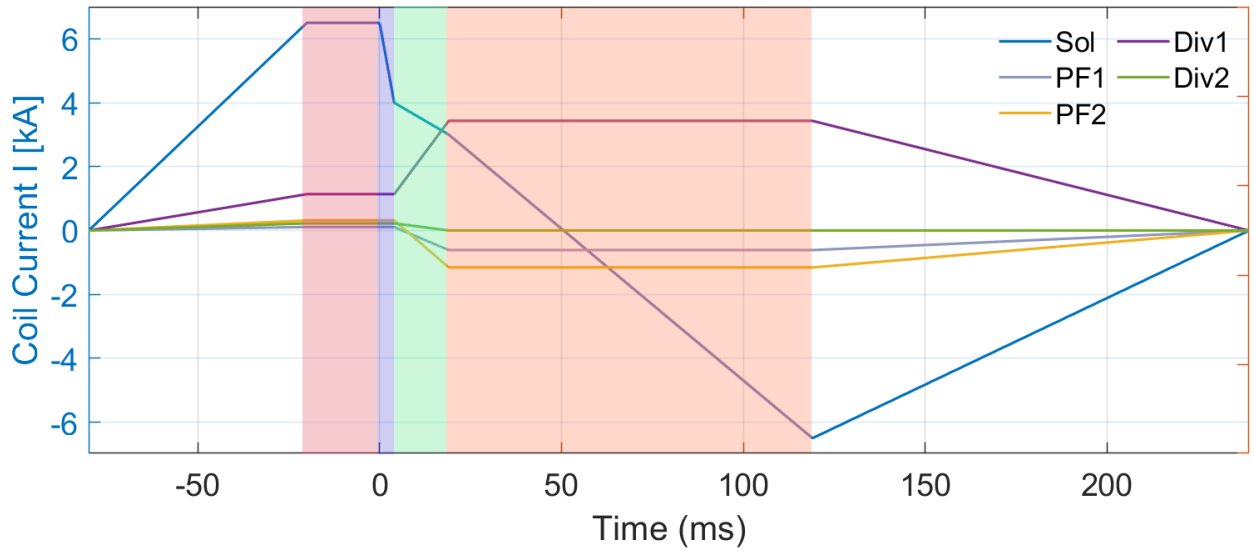

Figure 17: Control coils and solenoid current waveforms for the Spitzer resistivity model. The red area indicates the null-field period, the blue area indicates the breakdown ramp period, the green area indicates the PF & Div ramp period, and the orange area indicates the pulse period.

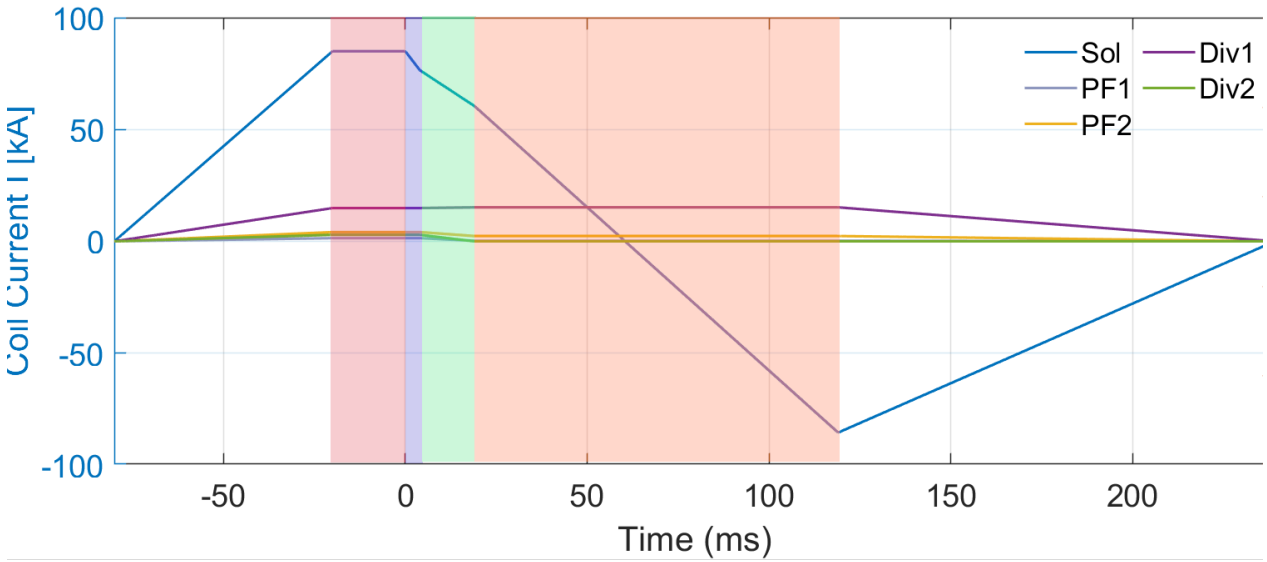

Figure 18: Control coils and solenoid current waveforms for the neoclassical resistivity model. The red area indicates the null-field period, the blue area indicates the breakdown ramp period, the green area indicates the PF & Div ramp period, and the orange area indicates the pulse period.

Solenoid waveform				
Time period τ (ms)	(-20, 0)	(0, 4)	(4, 15)	(15, 115)
I_{sol} (kA)	(85.5, 85.5)	(85.5, 76.5)	(76.5, 60.5)	(60.5, -85.5)
dI/dt (kA/ms)	0	2.25	1.067	146

Table 4: Input solenoid current, using the neoclassical model.

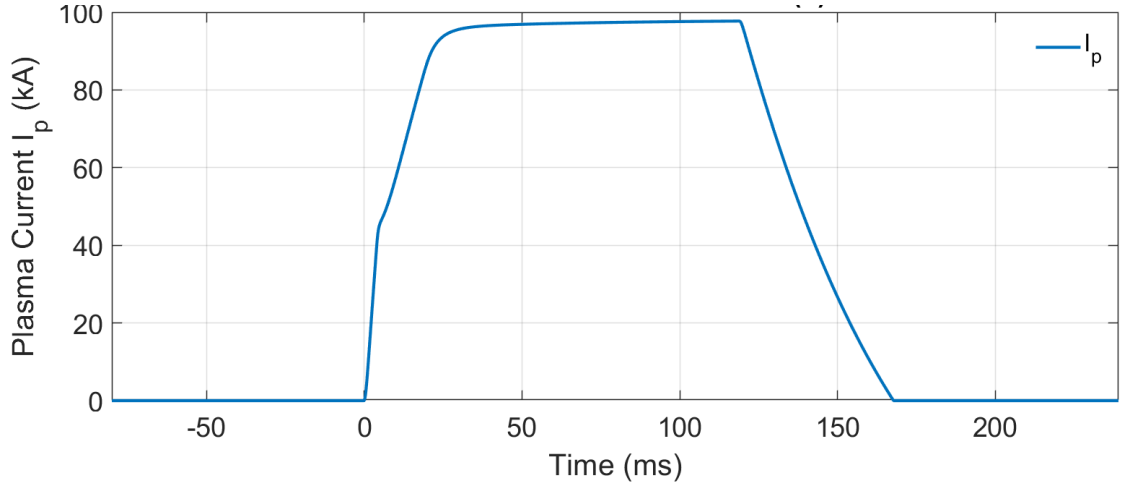

Figure 19: Spitzer resistivity

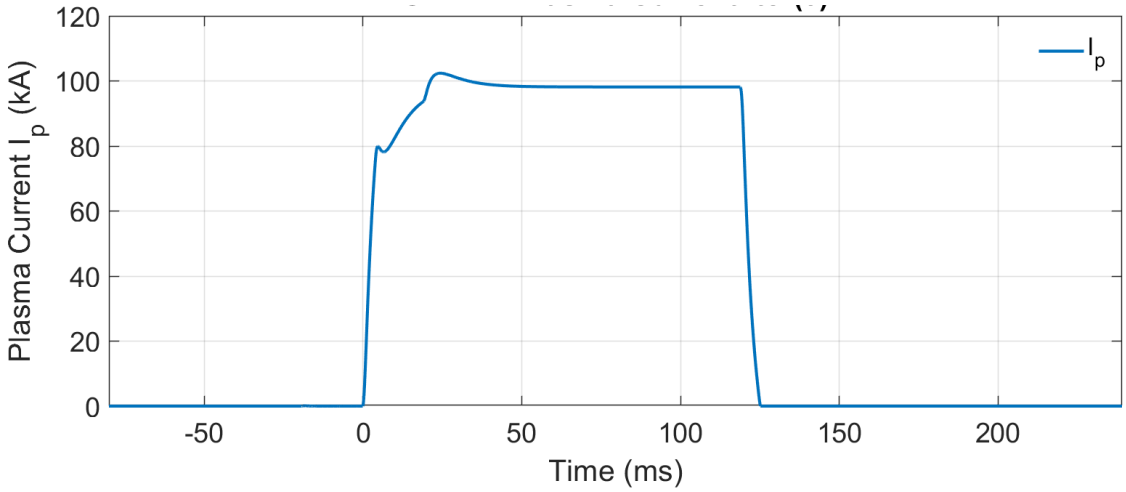

Figure 20: Neoclassical resistivity.

Figures 19 and 20 depict the simulated plasma currents for each model. In both cases the desired 100 kA are achieved and plasma breakdown occurs.

5 Conclusions

Including the neoclassical resistivity model in FIESTA has allowed valuable comparisons to be made with the results previously established by the Spitzer resistivity model. On the one hand, it has been shown that, for the working region targeted by the SMART tokamak experiments concerning the plasma aspect ratio, the neoclassical model predicts an increase in resistivity by one order of magnitude, which implies the need for a stronger central solenoid current. On the other hand, the new resistive model predicts an increase in magnetic poloidal flux and an augmented eddy current in the device vessel, resulting in higher currents in the control coils to stabilise the plasma. The generalised increase in SMART currents, predicted by recent FIESTA simulations, will lead to higher energy costs in future experiments on the device. However, although FIESTA is a robust tool, it still requires the implementation of other plasma phenomena.

Apart from the enriched resistivity from trapped particles, the neoclassical model gives other predictions, such as the bootstrap current. The bootstrap current's existence lessens the need for external current input, increasing the efficiency and economic viability of the fusion process. One possible future for FIESTA developers could aim to model this current inside the tokamak SMART. Furthermore, all simulations have been performed considering a constant temperature during plasma breakdown, which does not reflect reality. Plasma breakdown is a convoluted process where plasma temperature evolves. It is expected that, once these dynamics are implemented in FIESTA simulations, the difference between the solenoid current in both models will decrease.

The results conclude with the requirement of further development of FIESTA to obtain more realistic plasma equilibria simulations.

A Toroidal geometry. Description of a torus.

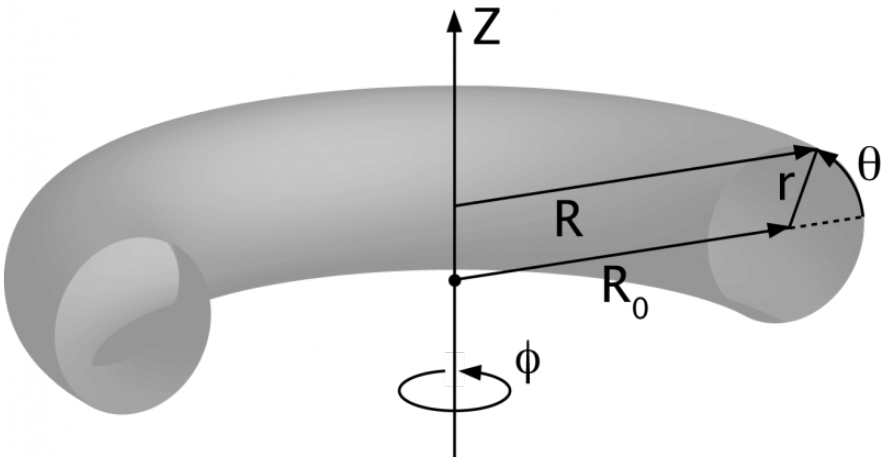

Figure 21: Toroidal coordinates. Source: [19]

In mathematics, a toroid is a surface created by revolving a curve or shape around an axis such that it forms a ring or donut-like structure with a hole in the middle. The axis of revolution passes through the central hole and does not intersect the surface of the toroid. In figure 21 the coordinates, commonly used in plasma, are depicted. These are a modification of the cylindrical coordinates, where R is the distance form the axis to the described point, R_0 is the major radius of the torus, r is the minor radius of the torus, θ is the poloidal angle, ϕ is the toroidal angle and Z is the axis of revolution.

B Plasma geometry

- **Plasma center**

  R_{geo} is defined as the radial position of the plasma center.

- **Plasma radius**

  $r_{geo} = a$.

- **Aspect ratio**

  $A = \frac{R_{geo}}{r_{geo}}$.

- **Geometric height**

  Z_{geo} is defined as the position of the plasma center in the Z-axis.

- **Elongation**

  $\kappa = \frac{Z_{max} - Z_{min}}{2r_{geo}}$.

- **Triangularity**

  $\delta = \frac{Z_{max} - Z_{geo}}{r_{geo}}$. This parameter can be positive or negative, depending on where the plasma is facing, the inner or the outer wall of the vessel.

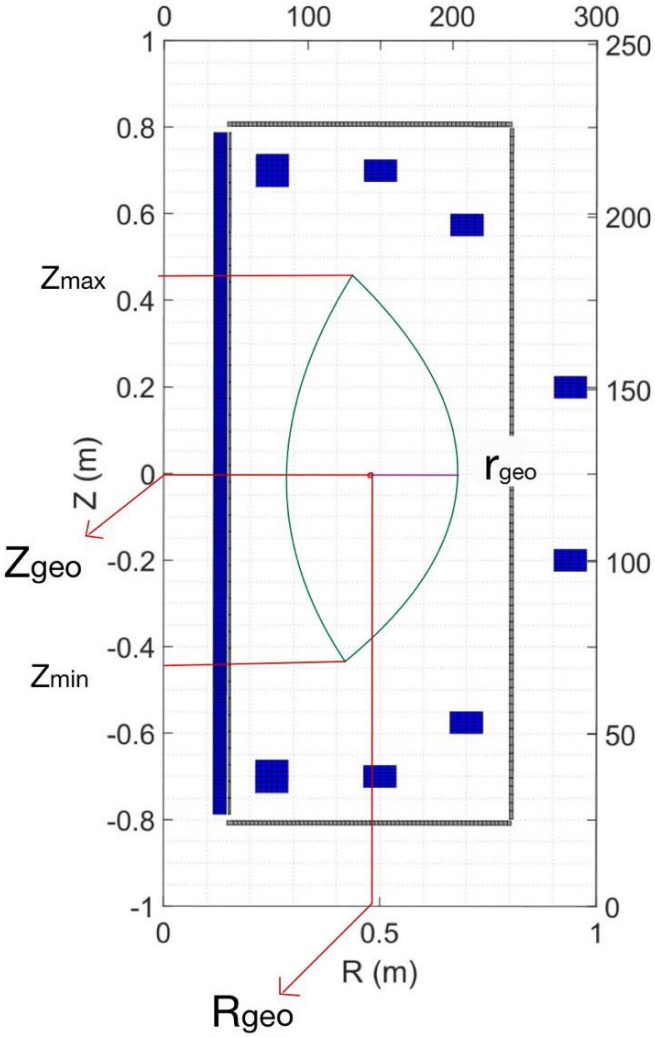

Bibliography

[1]F. Romanelli et al., 'Fusion electricity: A roadmap to the realization of fusion energy', EFDA (2012).

[2]IEA, 'World energy outlook 2022', CC BY 4.0 (report); CC BY NC SA 4.0 (Annex A) (2022).

[3]K. Heyde, *Basic ideas and concepts in nuclear physics: an introductory approach* (CRC Press, 2020).

[4]E. Gregersen, 'Nuclear binding energy', Britannica (2023).

[5]J. Wesson and D. J. Campbell, *Tokamaks*, Vol. 149 (Oxford University Press, 2011).

[6]J. P. Freidberg, *Plasma physics and fusion energy* (Cambridge University Press, 2008).

[7]F. F. Chen et al., *Introduction to plasma physics and controlled fusion*, Vol. 1 (Springer, 1984).

[8]R. Fitzpatrick, *Plasma physics: An introduction* (CRC Press, 2022).

[9]P. Ricci and D. Testa, *MOOC: Plasma physics: Introduction*, (EPFL, Switzerland), course, 2018.

[10]A. Piel et al., *An introduction to laboratory, space, and fusion plasmas* (Springer, 2010).

[11]U. Baldini, *Jet's power in radio-loud active galactic nuclei: A case study on the nature of blazar candidates*, (University of Padova, 2015).

[12]S. J. Doyle et al., 'Single and double null equilibria in the smart tokamak', Plasma Research Express **3**, 044001 (2021).

[13]S. Doyle et al., 'Magnetic equilibrium design for the smart tokamak', Fusion Engineering and Design **171**, 112706 (2021).

[14]B. Lloyd et al., 'Low voltage ohmic and electron cyclotron heating assisted startup in DIII-D', Nuclear Fusion **31**, 2031 (1991).

[15]J. P. Freidberg, *Ideal mhd* (Cambridge University Press, 2014).

[16]R. D. Hazeltine and J. D. Meiss, *Plasma confinement* (Courier Corporation, 2003).

[17]R. J. Goldston, *Introduction to plasma physics* (CRC Press, 2020).

[18]S. Hirshman et al., 'Neoclassical conductivity of a tokamak plasma', Nuclear Fusion **17**, 611 (1977).

[19]B. van Milligen, 'Toroidal coordinates', FusionWiki (2009).